Physics – Uspekhi **60** (5) 490 – 508 (2017)

PHYSICS OF OUR DAYS

PACS numbers: **62.50. – p**

Unusual plasticity and strength of metals at ultra-short load durations

G I Kanel, E B Zaretsky, S V Razorenov, S I Ashitkov, V E Fortov

DOI: https://doi.org/10.3367/UFNe.2016.12.038004

Contents

Abstract. This paper briefly reviews recent experimental results on the temperature-rate dependences of flow and fracture stresses in metals under high strain rate conditions for pulsed shock-wave loads with durations from tens of picoseconds up to microseconds. In the experiments, ultimate ('ideal') values of the shear and tensile strengths have been approached and anomalous growth of the yield stress with temperature at high strain rates has been confirmed for some metals. New evidence is obtained for the intense dislocation multiplication immediately originating in the elastic precursor of a compression shock wave. It is found that under these conditions inclusions and other strengthening factors may have a softening effect. Novel and unexpected features are observed in the evolution of elasto-plastic compression shock waves.

Keywords: shock waves in solids, high-rate straining, high-rate fracture, dynamics of dislocations, ideal strength, anomalous thermal hardening, polycrystalline metals and single crystals

G I Kanel, S I Ashitkov, V E Fortov Joint Institute for High Temperatures, Russian Academy of Sciences,
ul. Izhorskaya 13, 125412 Moscow, Russian Federation
E-mail: kanel@ficp.ac.ru, asi@iht.mpei.ac.ru, ashitkov@yandex.ru
E B Zaretsky Ben-Gurion University of the Negev,
8410501Beer-Sheva, Israel
E-mail: zheka@bgu.ac.il
S V Razorenov Institute of Problems of Chemical Physics, Russian Academy of Sciences,
prosp. Akademika Semenova 1, 142432 Chernogolovka,
Moscow Region, Russian Federation
E-mail: razsv@ficp.ru

Received 11 October 2016, revised 23 December 2016
Uspekhi Fizicheskikh Nauk **187** (5) 525 – 545 (2017)
DOI: https://doi.org/10.3367/UFNr.2016.12.038004
Translated by E N Ragozin; edited by A Radzig

1. Introduction

The development of new technologies for material processing, experimental techniques, and methods for atomistic computer simulations of inelastic deformation and fracture processes have fostered the growth of interest in the investigation of strength and plasticity of solids for extremely short loading durations. In particular, one of the promising avenues of precision material processing involves the employment of femtosecond lasers. As shown in our review, for so short a pulse duration, the resistance to deformation and fracture of solids exceeds by a few orders of magnitude the corresponding values at ordinary deformation rates and approaches the ultimate ('ideal') strengths. In our opinion, it is not at all indifferent for the optimization of technology to know that aluminum under short stressing may exhibit the same hardness as sapphire. Also unusual is the temperature effect on the flow stress of crystalline bodies, which sometimes turns out to be opposite in sign in comparison with ordinary conditions. In particular, this explains why some metallic materials are prone to developing deformation instability with the formation of adiabatic shear bands, while others are not.

Extreme states of matter are commonly associated with high pressures and temperatures [1, 2] which are experimentally achieved by substance compression in strong shock waves. The short duration of a shock-wave action is frequently regarded as a drawback of the method. On the other hand, the short duration of a mechanical load pulse provides the possibility of realizing exotic states of matter distant from equilibrium and studying the material behavior under extremely high deformation rates. Investigations into the temperature-rate dependences of the resistance to deformation and fracture of metals and alloys permit studying the main patterns of motion of plastic deformation carriers — dislocations — and revealing the governing factors and laws of the formation and development of material damage. This information is required for optimizing the regimes of mechanical material processing, as well as for solving high-velocity impact and penetration problems.

The results of research in this area have been generalized in a series of reviews and monographs; among recent ones, mention should be made of Refs [3–8]. Numerous measurement data have been published on the pressure dependence of flow stress under shock compression (see Ref. [9] and references cited therein), as well as in shockless (quasi-isentropic) compression [10, 11]. What is new is the determination of the stressed material state at different stages of elastoplastic shock compression using pulsed X-ray structural diagnostics [6, 12, 13]. Our review deals with the most exotic results obtained by the authors during the last decade. To discuss them, there is good reason to recall some of the foundations of modern notions about the mechanisms of high-rate deformation and fracture of solids.

In terms of dislocation theory, the plastic deformation rate $\dot{\gamma}$ is determined by the average motion velocity v_d of mobile dislocations and their density N_m, which are related by the Orowan formula

$$\dot{\gamma} = bN_m v_d \,, \tag{1}$$

where b is the Burgers vector. The average velocity of mobile dislocations is a function of stress, temperature, and the density of various defects which impede the dislocation motion, including the dislocations themselves. Apart from dislocations, of course, a significant contribution to the mechanism of plastic deformation can be made by twinning, which is especially important for crystals with hexagonal close-packed and body-centered cubic structures. However, this does not introduce in the majority of cases radical changes to the interpretation of rate and temperature dependences of flow stress under high-rate deformation of metals. The limited integral information about the laws of high-rate deformation acquired in experiments does not, as a rule, permit separating the contributions of different types of dislocations. This is the reason why in the subsequent discussion we will employ the dislocation terminology in some averaged and simplified sense, without going into the features of the high-rate deformation mechanism inaccessible to contemporary experiments. Modern physical plasticity theories also consider so-called disclination and rotation modes, which are sometimes invoked to describe strong plastic deformations; however, for the processes and phenomena discussed in our review, this is, in our opinion, an excessive complication.

It is well known that the flow stress of crystalline solids rises with increasing loading rate. For many metals, this dependence strengthens sharply when the deformation rate becomes higher than $\sim 10^3 - 10^4$ s^{-1}, which is attributed to a change in the mechanism of dislocation motion [4, 14]. For a low strain rate, dislocations overcome Peierls barriers and obstacles due to the combined action of the applied stress and thermal fluctuations. As a consequence, the increase in temperature is accompanied by a lowering of the material's yield strength. A higher stress is required for a high-rate deformation. For a sufficiently high strain rate, the working stress is so high that dislocations are capable of overcoming barriers and obstacles without the additional contribution from thermal fluctuations. In this case, the average dislocation velocity v becomes a linear or close-to-linear function of the applied shear stress τ and is controlled by drag forces of various natures in accordance with the following relation [15]:

$$Bv = b\tau \,, \tag{2}$$

where B is the dynamic drag coefficient, which includes the contributions made by obstacles, electrons, and phonons. The interaction of moving dislocations with electrons is believed to be significant only at a low temperature. At normal and elevated temperatures, the coefficient B_p of dislocation drag by a phonon gas (phonon friction or phonon viscosity) may be represented as a linear function of the temperature [16]:

$$B_p = \frac{k_B T \omega_D^2}{\pi^2 c^3} \,, \tag{3}$$

where k_B is the Boltzmann constant, ω_D is the Debye frequency, and c is the speed of sound.

An exhaustive discussion of the manifestations of phonon viscosity may be found in review [17]. Since the phonon viscosity is proportional to the temperature, one might expect a linear increase in flow stress with increasing temperature at a very high deformation rate [17]. At a sufficiently high stress termed ideal, or ultimate, shear strength, a material must lose stability relative to shear stress and may be deformed without any contribution from dislocations. The magnitude of ideal shear strength τ_{id} is proportional to the shear modulus G and, according to different estimates, ranges $\tau_{id} \approx G/10 - G/2\pi$. Since the shear modulus lowers with temperature, the ideal shear strength should also lower with heating. Figure 1 serves to illustrate the relative contributions of the thermofluctuational and over-barrier mechanisms of dislocation motion in relation to the temperature and deformation rate.

The second, and no less important, parameter that defines the resistance to plastic deformation is the total dislocation density. Figure 2 explains the dependence of the yield strength on the dislocation density. Defect-free crystals are characterized by the highest values of yield strength. Similar, or close to them, high-strength structural states are realized in metal whiskers that are micrometer-sized in thickness [18]. With the appearance of dislocations, the flow stress decreases rapidly to a minimum at the critical dislocation density N_c; with a further increase in density, the dislocations begin blocking each other, with the result that the flow stress becomes higher. The density of mobile dislocations rises in the course of plastic deformation.

Unlike a fracture under normal conditions, which proceeds by way of propagation of one or several cracks, the

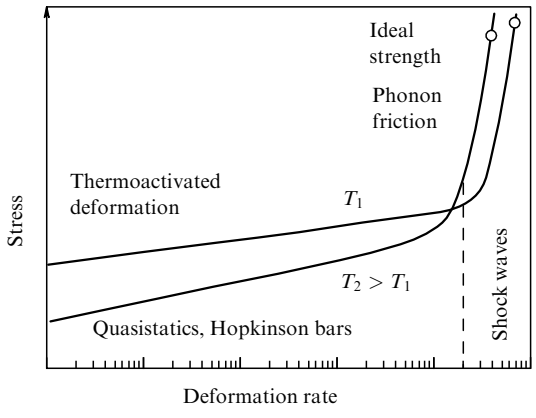

Figure 1. Approaching an explanation of the mechanisms of temperature-temporal dependences of yield strength.

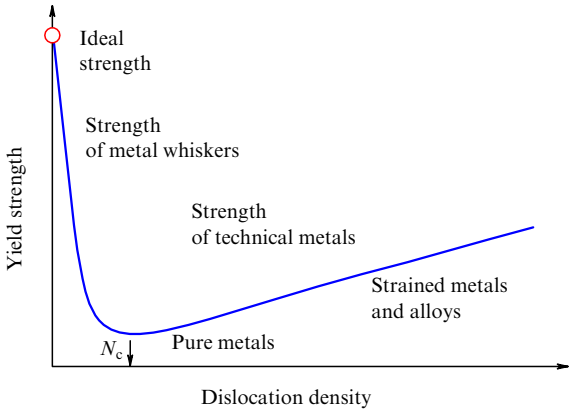

Figure 2. Graph of the dependence of the plastic flow stress of a crystalline body on the dislocation density [18].

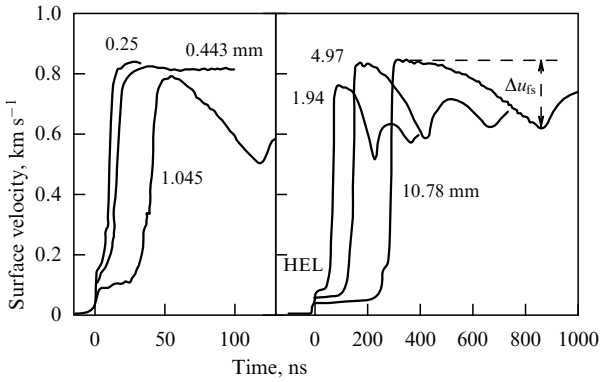

Figure 3. Results of measurements of free surface velocity histories for samples of Ma2-1 magnesium alloy [21]. The figures alongside the wave profiles indicate the specimen thicknesses.

high-rate fracture under ultrashort load pulse durations proceeds, owing to the lack of time for information exchange, by way of simultaneous nucleation, growth, and coalescence of a multitude of cracks or pores. Since the initiation and growth have a certain rate, the fracture stress rises with an increase in the tension rate. The values of fracture strength realized in this case are the result of competition of the growth of applied tensile stresses and their relaxation due to the appearance and growth of material discontinuity flaws. There is a maximum possible value of fracture stress: the ideal tensile strength, which corresponds to the vanishing derivative of the pressure with respect to the specific volume on the material's isotherm. The magnitude of ideal strength is found either by extrapolating the equation of state to the negative pressure domain or by *ab initio* calculations of compressibility. Remaining practically open is the question of possible polymorphous transformations in the negative pressure domain and their influence on the fracture strength.

Investigations of the mechanical properties of materials in the submicrosecond load duration range for deformation rates $> 10^3$ s^{-1} are carried out under shock-wave loading of the test specimens. These measurements are based on the fact that the wave structure and wave interaction dynamics are determined, apart from the thermodynamic equation of state of a substance, by elastoplastic deformation and fracture in the material [5, 7, 19, 20]. A great number of measurements are performed in the world with the use of this technique, which are accompanied by computer simulations of shock-wave phenomena by the methods of continuum mechanics and molecular dynamics [8]. Every two years, the American Physical Society holds large international conferences followed by the publication of 400 or more reports; every week, new research data are published in leading international journals. All these works are practically impossible to discuss or even mention in a journal paper. In our review, we present primarily the results of our own experimental investigations of the last decade, which are pioneering to one extent or another, stand out against the series of routine measurements in this area, are to an extent debatable, and attract the attention of scientists in related areas. We believe that all investigations outlined here lie in the mainstream of the development of this realm of science, because the formulation of problems aimed at studying the effect of structural factors, temperature, and impact duration is natural and inevitable.

In the experiments under discussion, a plane shock wave is in one way or another produced in the plate of investigated material, and the wave structure is measured at the output of a specimen — as a rule, by measuring the free surface velocity as a function of time. The thickness of the plane specimen, which defines the time of shock propagation, may vary from about 50–100 μm to 10 mm or more, while the free surface velocity history is measured with a resolution of 1 ns (10^{-9} s) with the use of modern experimental instrumentation. Quite recently, it became possible to stage experiments on specimens of micrometer and submicrometer thicknesses, with the temporal measurement resolution reaching the picosecond (10^{-12} s) level.

By way of example, Fig. 3 plots the histories of free surface velocity $u_{fs}(t)$ for plane specimens of an Ma2-1 magnesium alloy of various thicknesses, which were measured in Ref. [21] at room temperature. A shock compression pulse was produced in the specimens by the impact of a plate several times thinner than the specimen. Because of a sharp compressibility increase in transition from an elastic uniaxial compression to a plastic one, the shock wave loses stability and splits into an elastic precursor, which propagates at a velocity close to the longitudinal speed of sound c_l, and its following plastic shock wave, whose velocity is determined by the bulk compressibility of the material. The compression stress in the elastic precursor is equal to the Hugoniot elastic limit (HEL). From the measured velocity history of the free surface, the HEL magnitude is defined as

$$\sigma_{HEL} = \frac{\rho c_l u_{HEL}}{2}\,, \tag{4}$$

where u_{HEL} is the free surface velocity behind the elastic precursor front, and ρ is the material density. Although the term 'Hugoniot elastic limit' is universally accepted, strictly speaking, it is not quite correct, because the σ_{HEL} value is not a constant. One can see from the comparison of the wave profiles in Fig. 3 that, despite the growth of parameters behind the front of the elastic precursor in each wave profile, the stress at the elastic precursor front decreases as the wave propagates. This decay of the elastic precursor is a consequence of stress relaxation in the course of plastic straining immediately behind the elastic shock wave.

For the impactor-to-specimen thickness ratios employed in the experiments, the loading conditions near the free rear surface of the specimen in Fig. 3 correspond to the onset of

shock damping under the action of the overtaking rarefaction wave, whose approach to the surface is responsible for lowering the velocity. Only a part of the rarefaction wave limited by the value of dynamic tensile material strength is recorded in the free surface velocity history: tensile stress is generated inside the specimen after the reflection of the compression pulse from the free surface, resulting in its fracture — spalling. In this case, a relaxation of the tensile stress occurs and a compression wave (spall pulse) forms, whose approach to the specimen surface results in the second increase in its velocity. The velocity pullback $\Delta u_{\rm fs}$ in its decrease from the maximum to its value in front of the spall pulse is proportional to the fracture stress — the spall material strength under given loading conditions. The relationship used to determine the spall strength from the measured $\Delta u_{\rm fs}$ values results from an analysis of wave interactions by the method of characteristics; for elastoplastic bodies, this relationship is somewhat complicated by the necessity of taking into account different wave velocities. The subsequent oscillations of surface velocity result from multiple wave reflections inside the spalled layer of the specimen between its rear surface and the fracture surface. The period of velocity oscillations is determined by the spall thickness and the sound velocity.

2. Methodology of shock-wave investigations of the temperature-rate dependences of dynamic strength

There are two ways to directly acquire information about the relationship between plastic deformation rate and flow stress, which involve measurements of elastic precursor damping [22, 23] and measurements of the width of a plastic shock wave [24, 25]. High-rate fracture is studied by analyzing spall phenomena [26, 27]. These methods of investigation are briefly characterized below, and then the most interesting results will be presented. To gain additional information about the macrokinetic features of high-rate straining and fracture, computer simulations of shock-wave experiments are employed with the use of some hypothetical models and constitutive relations. This area requires special discussion and is not considered in our review.

2.1 Decay of elastic precursor and initial rate of plastic deformation

The decay of the elastic precursor of a shock compression wave due to stress relaxation is related to the rate $\dot\gamma_{\rm p} = (\dot\varepsilon_x^{\rm p} - \dot\varepsilon_y^{\rm p})/2$ of plastic deformation behind its front by the equation [22, 23]

$$\left.\frac{{\rm d}\sigma_x}{{\rm d}h}\right|_{\rm HEL} = -\frac{4}{3}\frac{G\dot\gamma_{\rm p}}{c_{\rm l}}\,, \tag{5}$$

where h is the distance traversed by the wave, G is the shear modulus, and $c_{\rm l}$ is the velocity of precursor front propagation, assumed under this approximation to be equal to the longitudinal speed of sound. Collected in Fig. 4 are experimental data, both our own and from the literature [28–34], on the elastic precursor damping in aluminum, including data in the picosecond pulse duration range obtained with film specimens about 1 μm in thickness. These measurements will be discussed separately in Section 3.2. The compression stress behind the precursor front, which is equal to the HEL of aluminum, varies, according to measurements, from 50 MPa at a distance of 10 mm to 20.5 GPa at a distance of 1.2 μm. We note that an elastic compression of up to 20.5 GPa is also realized in a steady plastic shock wave which has the same propagation velocity $U_{\rm S} = 7.8$ km s^{-1} at a final shock compression pressure of 38.7 GPa. So strong a compression results in a significant increase in the shear modulus in relation (5). Full symbols in Fig. 4 indicate normalized quantities $\sigma_{\rm HEL}G_0/G$ [30]. With this correction, the entire set of experimental data in Fig. 4 is described with reasonable accuracy by the empirical relation

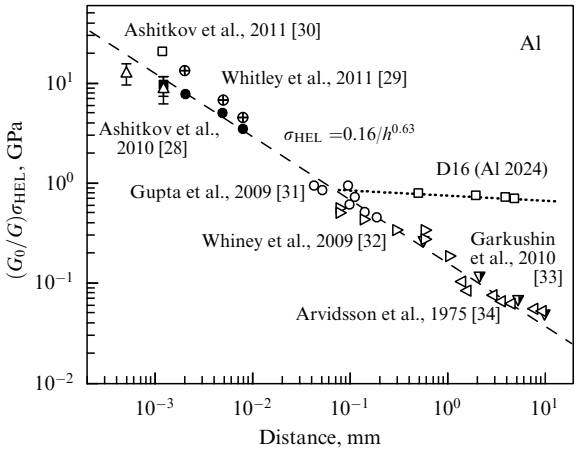

Figure 4. Dependence of the amplitude of an elastic shock wave in aluminum on the traversed distance [28–34]. Also shown for comparison are the data for D16 aluminum alloy.

$$\frac{G_0}{G}\,\sigma_{\rm HEL} = S\left(\frac{h}{h_0}\right)^{-\alpha}, \tag{6}$$

where $h_0 = 1$ mm, $S = 0.16$ GPa, and exponent $\alpha = 0.63$. For a compression stress below 1 GPa, which corresponds in Fig. 4 to distances longer than several dozen micrometers, the growth of the shear modulus is insignificant and will be ignored in the subsequent discussion. The maximum shear stress behind the precursor front is given by [19, 20]

$$\tau_{\rm HEL} = \frac{3}{4}\,\sigma_{\rm HEL}\left(1 - \frac{c_{\rm b}^2}{c_{\rm l}^2}\right) = \sigma_{\rm HEL}\,\frac{G}{E'}\,, \tag{7}$$

where $E' = \rho_0 c_{\rm l}^2$ is the longitudinal elasticity modulus. Eventually, empirical dependence (6) transforms, in view of expressions (5) and (7), into the dependence of the initial plastic deformation rate on the shear stress:

$$\dot\gamma_{\rm p} = \frac{3}{4}\left(\frac{\tau E'}{SG}\right)^{\alpha+1/\alpha}\frac{S\alpha c_{\rm l}'}{h_0 G}\,, \quad \text{or}$$

$$\dot\gamma_{\rm p} = 9.1\times 10^7\left(\frac{\tau}{\tau_0}\right)^{2.59}\,[{\rm s}^{-1}]\,, \tag{8}$$

where $\tau_0 = 1$ GPa. As is clear from the plots in Figs 5 and 6, the initial rate of plastic deformation behind the front of the elastic precursor decreases during its propagation from 10^9 s^{-1} at a distance of 1 μm to 10^3 s^{-1} at 5–10 mm, with the precursor damping subsequently decreasing sharply. We note that experiments with Hopkinson bars [35] demonstrate a sharp rise in the flow stress for a deformation rate of $\sim (2-5)\times 10^3$ s^{-1}.

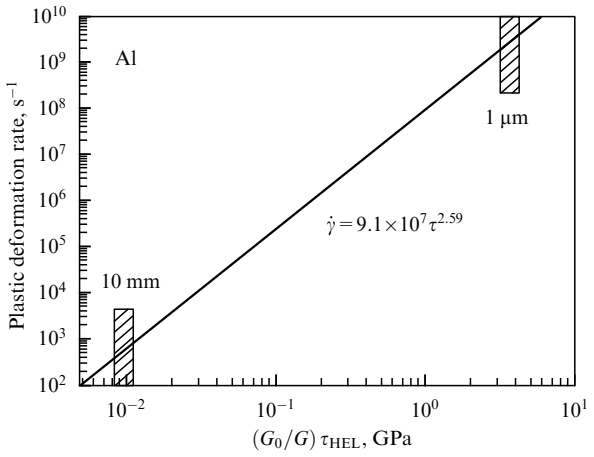

Figure 5. Shear stress dependence of the initial plastic deformation rate behind the elastic precursor front in aluminum calculated in accordance with relation (8) using the data from Fig. 4.

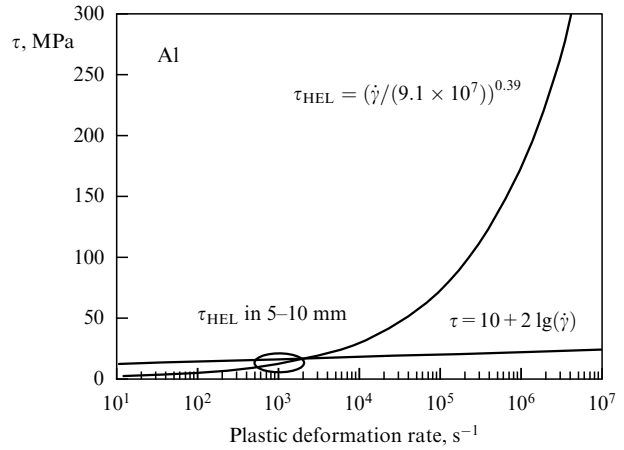

Figure 6. Flow stress of aluminum for moderate (logarithmic function [14, 35]) and high deformation rates.

Also shown in Fig. 4 are data on the decay of the elastic precursor in the D16 aluminum alloy. The stronger alloy exhibits a very weak decay of the elastic precursor in its propagation from 0.5 to 5 mm. In this range of traversed distances, the Hugoniot elastic limit of the alloy reaches about 0.71 GPa. In aluminum, this value of the stress behind the front of elastic precursor is realized at a distance of 92 μm, where the plastic deformation rate is $\sim 7\times10^5$ s^{-1}. It would appear reasonable that the alloy behavior would not be so much different from that of aluminum for specimens of smaller thicknesses.

2.2 Deformation rate in a plastic shock wave

The second source of data about material behavior under extremely high deformation rates is the compression rate in a plastic shock wave [24, 25]. In principle, the total deformation rate $\dot\varepsilon_x$ in a steady shock wave is defined quite simply: by differentiation of the corresponding portion of the history of particle velocity $u_p(t)$ and division by the wave propagation velocity U_S: $\dot\varepsilon_x = \dot u_p/U_S$. In the history of free surface velocity $u_{fs}(t)$, the recorded rise time in the plastic shock wave may be somewhat overestimated and the apparent deformation rate may be accordingly underestimated due to multiple reflections of the elastic wave between the free surface and the plastic front [5].

The determination of shear stress in a shock wave is not as unambiguous. The steady wave approximation implies the constancy of its shape and the constancy of the parameters of the substance state ahead and behind it, which generally does not quite correspond to experimental data. That is why the data discussed below should be regarded as estimative.

The total deformation rate $\dot\varepsilon_x$ is determined for the point of highest compression rate in the $u_{fs}(t)$ profile as $\dot\varepsilon_x = \dot u_{fs}/2U_S$. The highest shear deformation rate in the uniaxial compression, $\dot\gamma = \dot\varepsilon_x/2$, is the sum of elastic component $\dot\gamma_e = \dot\tau/2G$ and the rate $\dot\gamma_e = \dot\tau/2G$ of plastic shear deformation. Eventually, we have

$$\dot\gamma_p = \frac{\dot\varepsilon_x}{2} - \frac{\dot\tau}{2G}\,. \tag{9}$$

In a steady plane wave, the substance state varies along the Rayleigh line, which is a straight line $\sigma_x = -\rho_0^2 U_S^2 (V - V_0)$ connecting the states ahead of the wave and behind it. The deviator stress component in the wave is the difference between the stress σ_x in the Rayleigh line and the pressure p on the Hugoniot of the substance for the same compression ratio [24, 25]. In this case, the shear stress $\tau = (3/4)(\sigma_x - p)$ in the course of compression passes through a maximum at some intermediate point. At the maximum point, $\dot\tau = 0$ and $\dot\gamma_p = \dot\varepsilon_x/2$. The corresponding value of the shear stress is estimated as its value at the maximum point plus the value of shear stress ahead of the wave, which was determined in the same way as τ_{HEL}, though with the use of a higher value of the surface velocity in the middle of the portion of the wave profile between the precursor front and the plastic shock wave.

The values of shear stress τ and the deformation rate determined in this way from the experimental data of Ref. [21] for the Ma2-1 magnesium alloy are shown by a point in Fig. 7. The shock compression pressure in these experiments was equal to 3.8 GPa. The uncertainty in determining τ is primarily due to the absence of information about the stressed alloy state in the shock-compressed state. One can see from the plot in Fig. 7 that the rate of plastic deformation in the shock wave exceeds that in the elastic precursor by an order of magnitude for the same value of shear stress.

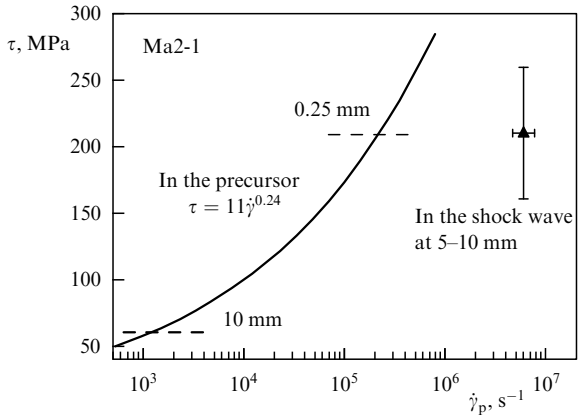

Figure 7. Relation between the plastic deformation rate $\dot\gamma_p$ and the shear stress τ behind the precursor front (solid line) and in the plastic shock wave (triangle) according to experimental data on the Ma2-1 magnesium alloy [21]. The dashed lines indicate the experimental range of elastic precursor parameters.

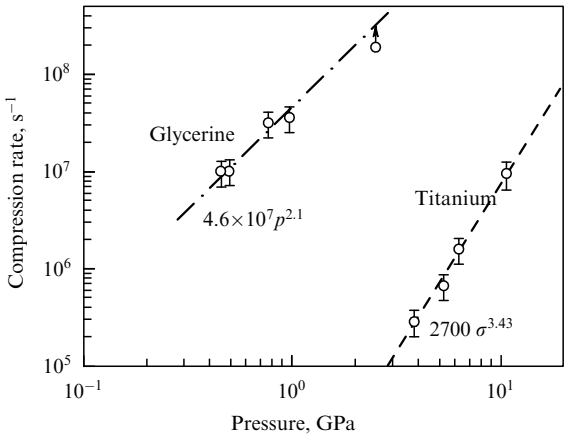

Figure 8. Compression rate in a shock wave as a function of shock compression pressure for titanium [36] and glycerin [37].

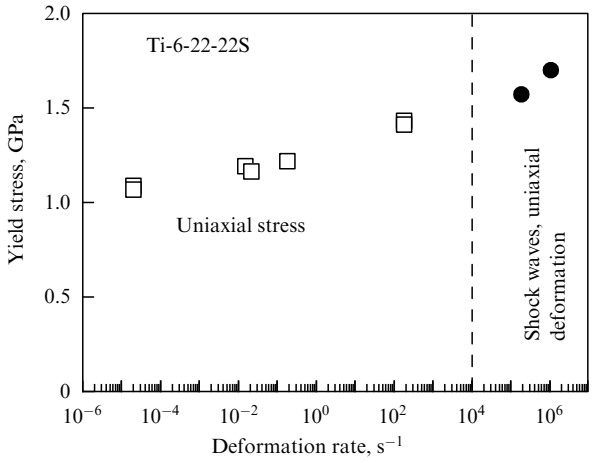

Figure 9. Yield stress of Ti-6-22-22S high-strength titanium alloy as a function of the deformation rate (using the data of conventional low-rate deformation measurements, measurements with Hopkinson bars for moderately high deformation rates, and shock-wave measurements [38]).

A similar relation between the deformation rates was also observed in experiments with the majority of other metals and alloys with different crystal structures. Most likely, such a fall in the characteristic material viscosity $\tau/\dot{\gamma}_p$ in the course of plastic deformation development is attributable to intense dislocation multiplication. In this connection, it is pertinent to discuss the empirical Swegle–Grady relation [25], which is still intriguing to many researchers. Having analyzed the measurement data for rise times in a plastic shock wave for different materials, Swegle and Grady found that all of them may be described with acceptable accuracy by power functions of the final shock compression pressure with the same exponent equal to 4.

The measured compression rates in the shock wave are compared for titanium and glycerol in Fig. 8. These data suggest that the dependence on shock compression pressure for a liquid is much weaker than for a solid. The reason for this difference is that the viscosities of liquids and solids are of different physical natures: the viscosity of liquids is determined by momentum transfer in the course of chaotic molecular motion, while the viscosity of crystalline solids is governed by the dislocation dynamics. In particular, the strong dependence of the compression rate in a shock wave on its intensity is supposedly the result of rapid dislocation multiplication in the course of high-rate plastic deformation.

2.3 Temperature effects

The effect of temperature and deformation rate on the dynamic yield stress in the shock-wave loading of relatively high-strength metals and alloys does not or hardly differs from the expectations based on the extrapolation of data obtained at lower deformation rates. The yield stress data for the Ti-6-22-22S high-strength titanium alloy [38] at different deformation rates obtained in various ways are summarized by way of example in Fig. 9. The data of shock-wave measurements, measurements by the Hopkinson bar method for moderate deformation rates, and conventional low-rate deformation measurements, by and large, are quite consistent and are described by the same logarithmic dependence. For the model illustrated in Fig. 1, this signifies the retention of the thermoactivated deformation mechanism corresponding to the low-rate branch of the common dependence. With increasing temperature, the dynamic yield stress of this alloy becomes lower.

An anomalous increase in the Hugoniot elastic limit with temperature has been observed for several metals and ionic crystals. This effect is illustrated in Fig. 10, which compares the free surface velocity histories of commercial aluminum specimens measured at normal and elevated temperatures [33]. Raising the temperature led to a significant rise in the amplitude of the elastic precursor and lengthened the build-up time of parameters in a plastic shock wave: from 3–5 ns at room temperature to 8–12 ns at 605 °C. We note that the increase in precursor amplitude is partly due to a lowering of the longitudinal speed pf sound and, accordingly, an increase in the Poisson ratio. The lowering of the longitudinal speed of sound under heating shows up in the wave profile, as well as in the shortening of the time interval between the precursor front and the plastic shock wave. However, the effect does not reduce to the lowering of the dynamic impedance of the material; calculations of the shear stress from the value of σ_{HEL} with the use of the elastic modulus for a given temperature confirm the anomalous rise of the flow stress with temperature under these conditions.

Figure 11 serves to compare the effect of temperature on the dynamic yield stress measured for titanium and its alloys [39, 40]. One can see that the anomalous rise of dynamic yield

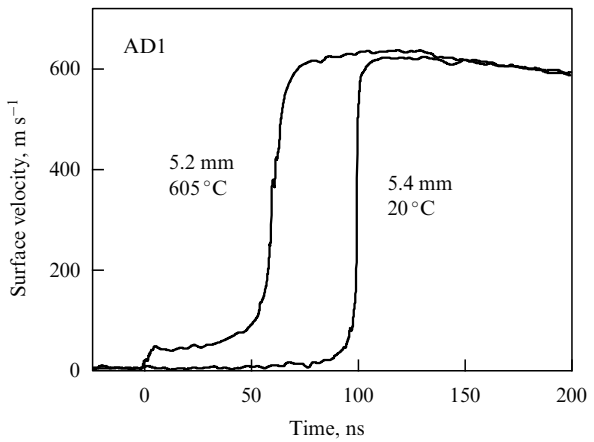

Figure 10. Initial portions of shock compression wave profiles for 5-mm thick aluminum specimens at temperatures of 20 and 605 °C [33].

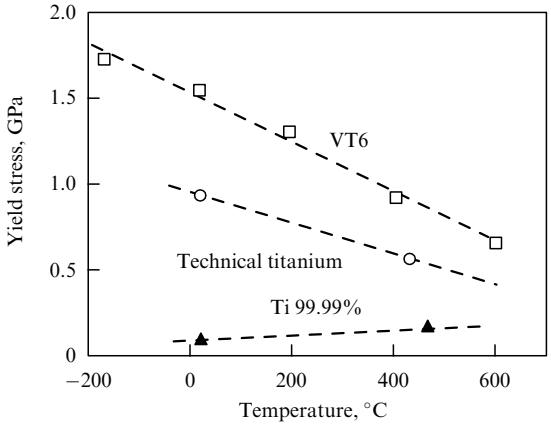

Figure 11. Temperature dependences of dynamic yield stress of titanium and its alloys from the data of shock wave measurements [39, 40].

stress upon heating takes place for pure titanium, where the high-rate plastic flow stress is comparable to the forces of phonon viscosity. The yield stress of alloys is heightened by artificially made obstacles for dislocation motion and far exceeds the dislocation drag stress due to phonon viscosity, with the result that anomalous thermal strengthening is not recorded for alloys.

2.4 Spall strength of metals

The spall strength of a material is calculated from the measured value of surface velocity decrease $\Delta u_{\rm fs}$ from its peak value in a compression pulse to the value in front of the spall pulse, as is illustrated in Fig. 3. The calculation is based on the analysis of the interaction of incident and reflected waves by the method of characteristics with the inclusion, where necessary, of elastoplastic material properties. In a linear approximation, the design equation is of the form [26, 41]

$$\sigma_{\rm sp} = \frac{1}{2}\,\rho_0 c_{\rm b}(\Delta u_{\rm fs} + \delta)\,, \tag{10}$$

where δ is the correction for the velocity history distortion due to the difference between the velocity of the spall pulse front and the velocity of the plastic part of the incident unloading wave in front of it. Such distortions occur when the stress relaxation in the fracture generates a compression wave in the material under tension, whose front propagates with the longitudinal speed of sound $c_{\rm l}$ and catches up with the plastic unloading part of the incident compression pulse moving with a bulk speed of sound ($c_{\rm b}$). The distortion is minimal for a triangular profile of the shock compression pulse at the instant it reaches the surface, which determines the optimal conditions for measuring its spall strength. High tensile stress is realized in the nanosecond and picosecond pulse duration ranges, and disregarding nonlinearity introduces large errors into its determination. In this case, in the processing of measurement data, use is made of shock adiabat extrapolation in the compression stress–particle velocity coordinates to the negative pressure domain, which leads to the relation

$$\sigma_{\rm sp} = \frac{1}{2}\,\rho_0\left(c_0 - \frac{b\Delta u_{\rm fs}}{2}\right)(\Delta u_{\rm fs} + \delta)\,, \tag{11}$$

where c_0 and b are the coefficients of the linear expression $U_{\rm S} = c_0 + bu_{\rm p}$ for the Hugoniot ($U_{\rm S}$ is the shock wave velocity, and $u_{\rm p}$ is the velocity of material particles behind the shock front).

The resistance to spall or the spall strength of a material characterizes the conditions of fracture initiation. As a fracture develops, the material 'weakens' by the growing discontinuities, and the process is completed at reduced stress. As is well known, for a short loading duration, the fracture, having begun, may not come to complete spalling, i.e., to a body division into parts. Completing the process requires additional expenses of energy which is consumed on growing discontinuity nuclei and plastic deformation of the material around them. This brings up the question of selecting spall criteria which would permit employing the data of a limited number of tests of a material to predict its reaction under arbitrary loading conditions.

In the 1960s–1970s, different empirical criteria were proposed, which defined the possibility and completeness of spalling in relation to the amplitude and duration of the acting pulse of a shock loading or the energy store in the spallable plate. However, these criteria do not take into account the real history of loading with stress relaxation in the course of fracture and are not very compatible with the algorithms for computer simulations of shock-wave phenomena. Although criteria of this kind have been proposed even up to the present time, in Refs [42–45], instead of finite criteria, the use of kinetic relations defining the fracture rate as a function of the current value of tensile stress, the attained fracture degree, and other parameters of state was proposed at the beginning of the 1970s and in the 1980s. Under this approach, the spall strength in some way characterizes the stress, whereby the growth of discontinuities compensates for the increase in tensile stress in the course of wave interactions.

Methodical issues and the factors defining the resistance to spall fracture of metals and alloys, ceramics and glasses, and single crystals and liquids are discussed at length in Refs [26, 27]. Here, we outline the results of research carried out in recent years.

A multitude of measurements dealing with spall strength were made for commercial metals and alloys to characterize their capacity to withstand a high-rate impact or an explosion. On the other hand, shock-wave measurements may also furnish new information on the ultimate material strength, the kinetics of fracture and the mechanism of its initiation and growth, and the topology and statistics of potential fracture nuclei, and may be of independent interest from the standpoint of materials science. This is the reason why recent research around the world is largely concerned with the quest for correlation between the structure of materials and their resistance to fracture in a wide range of deformation rates and temperatures.

The experimental data from Refs [28, 33, 46–48] on aluminum spall strength are collected in Fig. 12. The data are represented in the form of the relation between the spall fracture stress and the deformation rate, which is used in reference to the rate of substance expansion in a rarefaction wave defined as

$$\frac{\dot V}{V_0} = -\frac{\dot u_{\rm fsr}}{2c_{\rm b}}\,, \tag{12}$$

where $\dot u_{\rm fsr}$ is the measured rate of the decrease of the free surface velocity of a test specimen in the unloading part of a shock compression pulse. It was shown in Refs [49, 50] that the initial growth rate of the relative volume of discontinuities

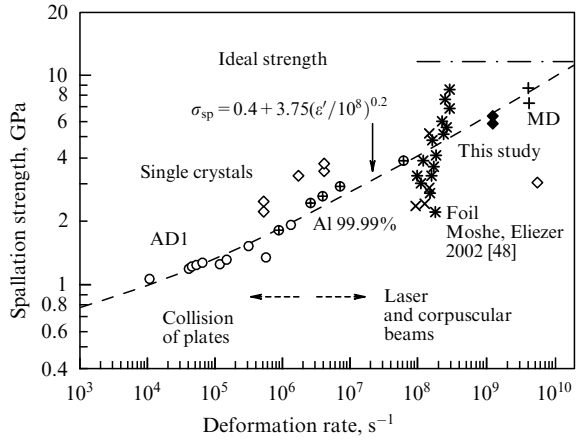

Figure 12. Measured spall strength of aluminum of various purity in comparison with the data for single-crystalline aluminum, results of spalling simulations by molecular dynamics, as well as the value of the ideal strength of aluminum from *ab initio* simulations.

in the spalling is equal, correct to a constant factor of $\sim (2-4)$, to the thus calculated rate of substance expansion in the unloading wave. This signifies that the dependence of spall strength on the so-defined deformation rate may be simply transformed to the stress dependence of the fracture rate [51].

The resistance to spall fracture of single crystals is higher than for polycrystalline aluminum and aluminum alloys. Polycrystalline materials contain relatively large stress concentrators, like intergrain boundaries and inclusions. These defects lower the stress level required to initiate fracturing. The high bulk strength of single crystals is evidently caused by their high homogeneity. Figure 12 also shows the results of atomistic simulations [52, 53] of high-rate fracture and spalling and of first-principle simulations [54] of 'ideal' aluminum strength. Extrapolation of experimental data to higher deformation rates shows their agreement with molecular dynamics simulations and predicts the attainment of an ideal strength for a tensile rate of about 2×10^{10} s^{-1}.

Increasing the temperature results in falling off the spall strength. Both for polycrystalline metals and for single crystals, the lowering of dynamic strength on heating to ~ 0.9 of the melting point T_m is considerably smaller than is the case for low deformation rates; on a further increase in temperature and its approach to the melting temperature, the decrease in spall strength becomes faster. In this case, single crystals and high-purity polycrystalline metals retain their high strength practically up to the melting temperature, which signifies the intersection of the melting phase boundary in the negative pressure domain. To state it in different terms, superheated crystal states are realized in pure metals under high-rate tension in these conditions. Commercial polycrystalline metals lose their resistance to fracture almost completely as the temperature approaches T_m [46, 55].

As is well known, the melting of alloys begins at a so-called solidus temperature and ends up at a higher liquidus temperature. The data of experiments [56] on the 6061 aluminum alloy suggest that the alloy does not lose its shear and bulk dynamic strength immediately at the onset of melting on crossing the solidus line. With increasing temperature and, accordingly, melt fraction, the spall strength of the 6061 alloy lowers gradually and becomes equal to zero only for a 20% content of the liquid phase. Although there is no obvious similarity in the behavior of commercial aluminum and aluminum alloys, one may assume the existence of small domains at the grain boundaries with a higher impurity density, where melting may commence even when the temperature is below the solidus temperature and rapidly lowers the resistance to spall fracture.

Liquids, like solids, possess resistance to uniform tension, i.e., tensile strength, which manifests itself, for instance, in cavitation. Quite recently, it has been possible to measure the spall strength of melt metals both in the submicrosecond duration range of impact load [57, 58] and in the picosecond range [59]. For relatively long times, it turns out that the spall strength of liquid tin, lead, and zinc is an order of magnitude lower than the strength of these metals in the solid state and amounts to a far smaller fraction of the ideal strength than is the case for water [60] and other liquids at room temperature. In the picosecond range, the spall strength of molten tin amounts to 1.9 ± 0.3 GPa, i.e., less than 30% of its ideal strength. For metals in the solid state, the spall strength measured in this duration range usually exceeds 70% of the ideal strength.

2.5 Approach to ultimate (ideal) strength

Let us consider the features of metal behavior for an ultrashort loading by the example of iron. Figure 13 shows the profiles of free surface velocity of iron film of thickness 250 ± 5 and 540 ± 5 nm measured in their irradiation by 150-fs long laser pulses with an energy density of 3 J cm^{-2} at the center of the focal spot [61]. Measured in the experiment was the displacement of the free rear specimen surface as a function of time by an interferometric technique with the use of frequency-modulated diagnostics with a resolution of about 1 nm in displacement, and 1 ps in time. The surface velocity histories were then obtained after several iterations to attain the best fit of the velocity integral to the measured history of surface displacement. The resultant velocity error is estimated at about 10%. The velocity of propagation of the wave configuration front in the range from 250 to 540 nm amounted to $U_S = 6.45 \pm 0.2$ km s^{-1} on average over all experiments. In this case, the surface velocity behind the first shock wave decreases from 1.06 ± 0.06 km s^{-1} at a distance of 250 nm to 0.45 ± 0.03 km s^{-1} at a distance of 540 nm. The high wave propagation velocity and the short rise time are indications that the first wave in the two-wave configuration is the elastic precursor. The compression stress behind the

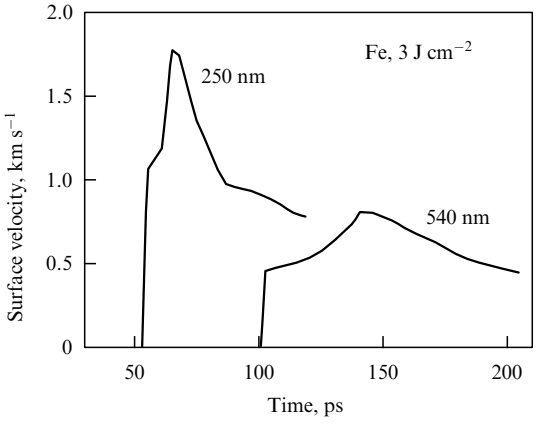

Figure 13. Time evolution of the compression pulse generated in iron film specimens by a laser pulse in the femtosecond range.

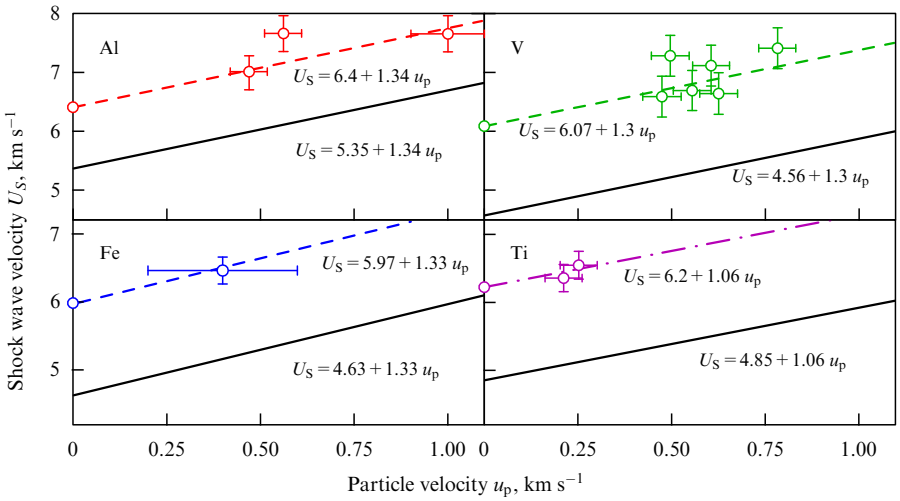

Figure 14. Results of measurements of the propagation velocities U_S and particle velocities u_p behind the front of the elastic precursor in thin films of aluminum [28], iron [65], and vanadium [66] in comparison with equilibrium adiabats and metastable shock adiabats of elastic compression calculated under the assumption of a constant Poisson's ratio. The authors' demonstrated data on the velocity of elastic shock waves in titanium are under preparation for publication.

precursor front amounted to 27.5 ± 2.5 GPa at a distance of 250 nm, and to 11.0 ± 1 GPa at 540 nm. We note for comparison that the Hugoniot elastic limit for sapphire in the submicrosecond time domain ranges from 13 to 24 GPa [62], depending on the direction of compression, and that the Hugoniot elastic limit of diamond amounts to 50–100 GPa [63–64].

For so high a stress of elastic uniaxial compression we may no longer restrict ourselves to the approximation of a constant elastic modulus and a constant speed of sound. In analyses and computer simulations, it would be convenient to have a description of strong elastic compressions based on some simple assumption which corresponds to experimental data with a reasonable accuracy. As shown earlier [67], the natural approximation for estimating the longitudinal speed of sound based on the assumption of a constant Poisson's ratio agrees nicely with available experimental data for metals in a broad range of shock compression pressures. The constancy of Poisson's ratio signifies the constancy of the longitudinal-to-bulk speeds of sound ratio c_l/c_b. Using a quasiacoustic approximation [20, 67] for the bulk speed of sound c_b, it may be shown that the ratio $c_l(V)/c_b(V)$ turns out to be the same both for the equilibrium bulk Hugoniot and for the metastable uniaxial Hugoniot only when coefficient b in the linear relationship between the shock wave velocity (U_S) and the particle velocity behind it (u_p), $U_S = c_0 + bu_p$, is of the same magnitude for both shock adiabats. The validity of this approximation is illustrated in Fig. 14 by the example of four metals under investigation.

Figure 15 depicts the corresponding diagram of iron states realized in the picosecond range of load durations, which shows the equilibrium shock adiabat of iron with a transition to the high-pressure ε phase, the metastable $p(V)$ adiabat of the low-pressure α phase, and the metastable uniaxial elastic Hugoniot. From the departure of the state behind the precursor front from the equilibrium adiabat of the low-pressure phase, it was possible to determine the maximum shear stress τ using the relation [19, 20]

$$\sigma_x(V) - p(V) = \frac{4}{3}\,\tau\,, \qquad (13)$$

where σ_x is the longitudinal elastic compression stress. The resultant values of τ were equal to 7.9 and 3.3 GPa.

The ultimate values of the shear strength — the ideal shear strength obtained from *ab initio* simulations — amount to 7.2–7.5 GPa for iron [68, 69]. The estimates from the data presented here yielded a maximum value of $\tau = 7.9$ GPa, which is even higher that the calculated ideal shear strength. However, it should be taken into account that both the shear modulus and, accordingly, its proportional ideal shear strength increase on compression. Anyway, it is valid to say that stressed states of iron quite close to ideal strength values were realized and measured in the picosecond load duration range.

Unfortunately, the significant nonstationarity of waves and the high rate of relaxation processes do not permit estimating the behavior of the material state after exceeding the Hugoniot elastic limit. In our experiments, we did not obtain convincing evidence for the $\alpha \to \varepsilon$ polymorphic transformation in the picosecond time range. The results of measurements of the free surface velocity histories of thicker iron specimens (1.2–1.6 μm) are indicative of the possibility

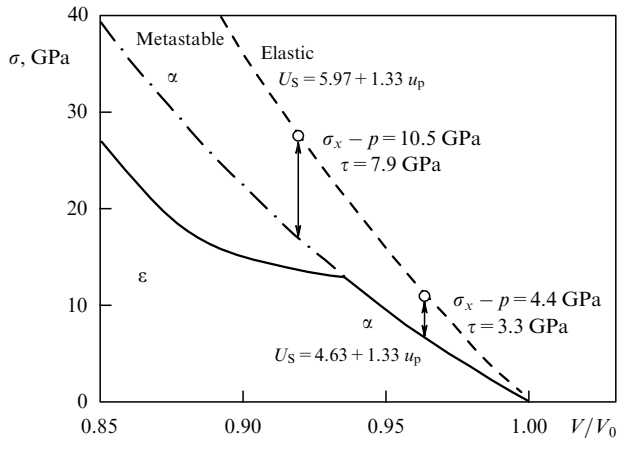

Figure 15. Parameters of the iron state behind the elastic precursor front at distances of 250 and 540 nm [65].

of the polymorphic transformation in a time on the order of 100 ps [70].

To date, measurements of the Hugoniot elastic limit and spall strength near their ultimate values have been made for fcc (face-centered cubic) [28–30], bcc (body-centered cubic) [65, 66, 70], and hcp (hexagonal close-packed) structure metals. Systematic measurements of the evolution of elastoplastic shock compression waves in the submicrosecond duration range were performed for the same metals. The totalities of experimental data, as a rule, are reasonably consistent and provide the basis for constructing wide-range models of high-rate straining. Experimental data in the picosecond range are also required for formulating and testing problems in atomistic simulations of deformation and fracture processes.

3. Temperature-rate dependences of the resistance to metal straining

In the framework of the program of determination of the temperature-rate dependences of resistance to high-rate deformation and fracture of metal materials, measurements were made of the evolution of elastoplastic shock compression waves in metals of different crystal structures at normal and elevated temperatures. The foundation was thereby laid for generalizing and estimating the contribution of different factors and for constructing constitutive relationships. Pure metals, metals of commercial purity, alloys, as well as single crystals of metals were investigated. In our review, we outline only the most interesting and unexpected results; more comprehensive data may be found in original papers. The test temperature was varied by heating for 5–15 minutes the specimens immediately prior to experiments using a resistive heater. The heating was or might be attended by a variation of the defect metal structure. Since there is good reason to compare, at different temperatures, the behavior of materials with about the same defect content, the majority of experiments were made on annealed samples. In doing so, it became clear that the effect of preliminary annealing on the resistance to high-rate deformation and fracture is not quite trivial and deserves special discussion.

3.1 Effects of annealing and mechanical hardening

It is well known that the annealing of a metal after its rolling or other kind of intense plastic deformation lowers its dislocation density and results in a lowering of the yield stress. This, however, is not always true for high-rate deformation under submicrosecond shock-wave loading. Figure 16 illustrates the difference among the annealing effects for pure copper [71] and tantalum [72]. While the HEL of copper lowered several-fold upon annealing, annealing tantalum and other bcc metals resulted in an increase in HEL. Figure 17 demonstrates the effect of annealing of commercial titanium [73], which has an hcp structure; both the Hugoniot elastic limit and the shape of the elastic precursor on the wave profile changed in this case. The formation of a peak on the frontal part is supposedly due to intense multiplication of dislocations [5] or their deblocking from the cloud of impurities. In principle, this observation is not at variance with the existing notions about the correlation between the flow stress and the dislocation density, which was discussed in the Introduction. We note once again that the hardness of all the metals under discussion lowered upon

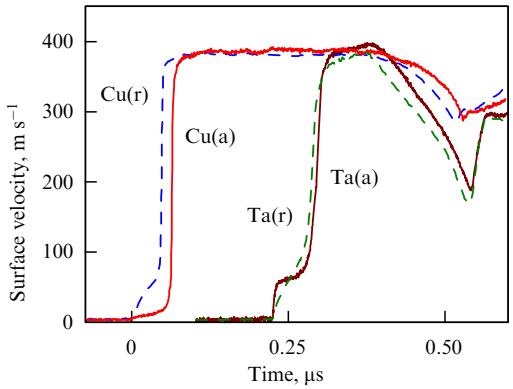

Figure 16. Free surface velocity histories of two-millimeter plates of copper [71] and tantalum [72] in the after-rolling state (dashed lines, index 'r') and after annealing (solid lines, index 'a').

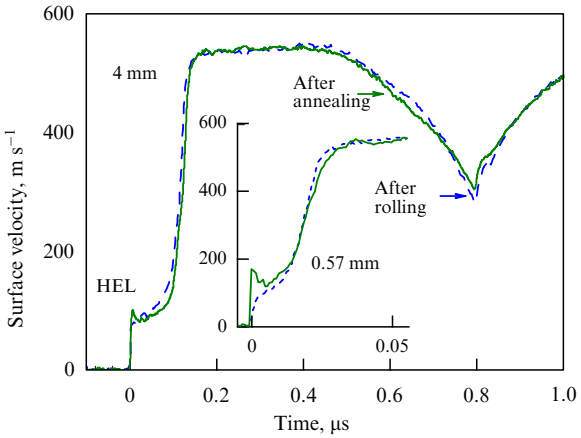

Figure 17. Free surface velocity histories of rolled (dashed lines) and annealed (solid lines) specimens of VT1-0 commercial titanium 4 and 0.57 mm in thickness [73].

annealing. Consequently, the 'critical' dislocation density, whereby the flow stress assumes its minimal value, is different for various deformation rates.

One can see from the presented examples of wave profiles that annealing not only changes the Hugoniot elastic limit but also lengthens the time interval between the elastic and plastic waves. This effect is shown in greater detail in Fig. 18, which compares the results of measurements in Ref. [72] of this interval in relation to the distance traversed by the wave for rolled and annealed tantalum. For distances $h < 1$ mm, the recorded velocity of the plastic shock wave turns out to be equal to the bulk speed of sound c_b in tantalum, although it must be higher than that according to the theory. In some other cases, the recorded velocity of the plastic shock wave may even be lower than the speed of sound [74]. The subsonic velocity of the plastic shock wave is often associated with the loss of shear strength in the course of shock compression [75, 76]. However, this interpretation may be true only for steady waves; the plot in Fig. 18 is more likely indicative of establishing the stationarity of the elastic and plastic waves. Transient processes in relaxing media call for a more intricate analysis, which has yet to be performed.

The observations of the anomalous effect of annealing on the dynamic yield stress correlate with the results of investigations of the effect of comminution of grain structure size by

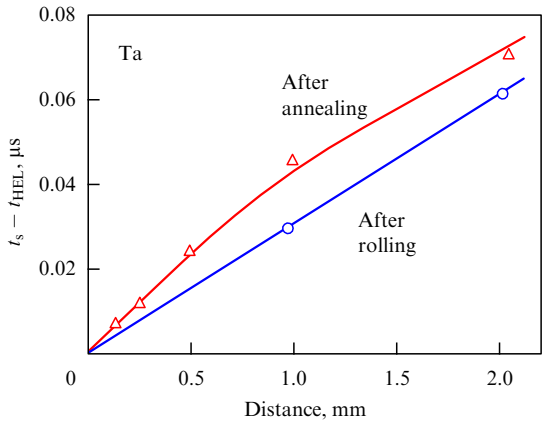

Figure 18. Time intervals between the elastic and plastic waves in tantalum in the states after rolling and after annealing as functions of the traversed distance.

the method of severe plastic deformation [77, 78]. While this processing is always attended by a significant increase in material hardness, the results of flow stress measurements in the submicrosecond range of load duration are not so unambiguous. For aluminum alloys, the increase in dynamic yield stress with a decrease of grain size is in a reasonable agreement with the data of low-rate measurements; for VT1-0 titanium and tantalum specimens, a small decrease instead of an increase occurs in dynamic yield stress; for copper, iron, and the VT6 titanium alloy, the effect is considerably weaker than under conditions of low-rate deformation.

By way of example, Fig. 19 compares the results of measurements [78] of free surface velocity histories $u_{fs}(t)$ for initial coarse-grain (CG) and submicrocrystalline ultrafine-grain (UFG) tantalum specimens. Their hardnesses are equal to 76–79 and 103–104 HRB units (hardness on scale B), respectively, i.e., intense plastic deformation resulted in a 30% increase in hardness. From the experimental data shown in Fig. 19, one can nevertheless see that the Hugoniot elastic limit σ_{HEL} after severe reduction of the grain size turned out to be even somewhat lower than for the initial coarse-grain material. This difference is especially pronounced in experiments on specimens ~ 0.65 mm thick. The effect is explained by a higher stress relaxation rate in the fine-grain material. The faster stress relaxation in the fine-grain material also manifests itself in a higher compression rate in a plastic shock wave.

The data from the experiments performed are an unambiguous demonstration of the anomalous effect of strengthening mechanical processing on the resistance to high-rate deformation and fracture. Phenomenologically, the lowering of dynamic yield stress in compression after rolling might be identified as a manifestation of the Bausinger effect, according to which a certain fraction of plastic deformation is reversible and does not make a contribution to deformation strengthening [79]. In favor of the Bausinger effect is a great deal of data on entire stress pulses [20], which suggest that the deformation process in the unloading after a shock compression deviates from the elastoplastic one towards lower deviator stresses, and that plastic deformation quite frequently begins immediately behind the unloading wave front without a finite elastic portion. A different interpretation proceeds from the assumption that structure imperfections may serve not only as obstacles to the motion of dislocations and twins, but also as their sources for high stress, thereby weakening the dependence of the yield stress on the deformation rate.

To understand the results of the performed experiments, account should obviously be taken of the fact that the applied shear stress gives rise not only to displacement of dislocations, but also to their generation and multiplication. The dislocation initiation takes place near stress concentrators, which are long-range crystal disorders. Structure imperfections, on the one hand, are a strengthening factor, but, on the other hand, are sources of plastic deformation carriers (dislocations). In other words, the same defects may determine enhanced resistance to deformation under quasistatic conditions and be the sources of plastic deformation carriers — dislocations — at high deformation rates and, accordingly, high stresses, and may thereby lower the resistance to plastic deformation. From the data outlined above, it follows that the differences among the rate dependences may be so strong that the effect of these defects on the flow stress may change sign in going from a quasistatic loading to the high-rate one.

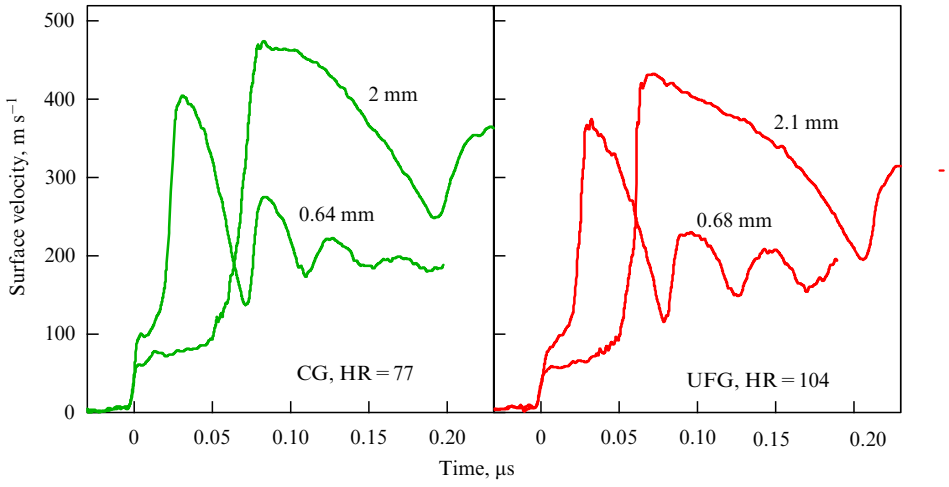

Figure 19. Results of measurements [78] of free surface velocity histories of initial (CG) and submicrocrystalline (UFG) tantalum specimens. The figures alongside the histories indicate sample thicknesses. HR — measured Rockwell hardness.

3.2 Temperature-rate dependences of flow stress at different stages of shock-wave deformation of metals

Figure 20 presents experimental data [80] on the temperature-rate dependence of the flow stress of high-purity aluminum in the 10^4-10^6 s^{-1} deformation rate range, obtained from measurements of elastic precursor decay and the plastic shock wave width at temperatures up to the melting point. As can be seen from Fig. 20, in particular, for the same shear stress the plastic deformation rate rises by at least an order of magnitude upon deformation in the shock wave, which amounts to $\sim 2\%$. In the elastic precursor, the shear stress $\tau_{\rm HEL}$ is related to the plastic deformation rate $\dot\gamma$ by the formula

$$\tau_{\rm HEL} = A\dot\gamma^{\,\alpha/\alpha+1}, \qquad (14)$$

where $\alpha = 0.88-1.148(T/T_{\rm m}) + 0.598(T/T_{\rm m})^2$ is the exponent in empirical relation (6) for precursor decay, which varies from 0.33 to 0.6 ($T_{\rm m} = 934$ K is the melting temperature of aluminum), and the coefficient A increases linearly with temperature: $A = 0.0155 - 4.07$ for the following dimensionalities of the stress, [MPa], and deformation rate, [s^{-1}]. In other words, the initial rate of plastic deformation behind the front of the elastic precursor increases approximately in proportion to the third power of the stress.

In Fig. 21, the flow stress in the elastic precursor from Fig. 20 is represented in the form of its temperature dependence for three fixed values of the plastic deformation rate. The linear form of these dependences is consistent with the phonon viscosity mechanism of dislocation drag. On the other hand, the strong stress dependence of the initial plastic deformation rate is at variance with the phonon viscosity mechanism at the mobile dislocation density corresponding to the initial state of the material.

The rate of plastic deformation is related to the mobile dislocation density and the average velocity of dislocations by the well-known Orowan formula (1). The mobile dislocation density of 10^7-10^9 cm^{-2}, which is required to provide the observed initial velocities of plastic deformation, exceeds the ordinary total dislocation density of 10^6-10^7 cm^{-2} in annealed pure metal. Consequently, to describe the high-rate deformation in dislocation terms involves assuming their intense nucleation or multiplication under the stress applied. Similar results were obtained for silver [74] and copper [71], which also possess an fcc structure. Molecular dynamics

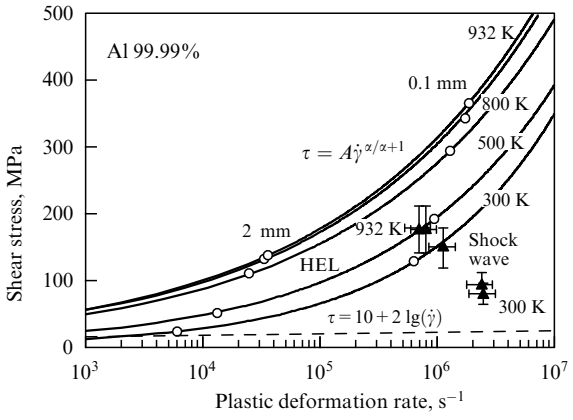

Figure 20. Dependences of the initial flow stress (lines) and the flow stress after a 2% deformation (points) on the plastic deformation rate and temperature for high-purity aluminum.

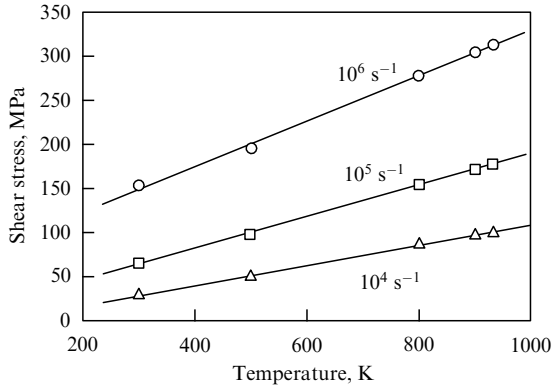

Figure 21. Temperature dependences of the initial flow stress in pure aluminum for three fixed plastic deformation rates. The linear character of the dependences is consistent with the phonon mechanism of dislocation drag.

simulations of dislocation motion in fcc metals [81, 82] confirm that the stress required to maintain dislocation velocity grows significantly with temperature, which is attributable to an increase in phonon viscosity; the mechanisms of rapid dislocation multiplication are not quite clear.

In contrast, bcc metals (iron [83], tantalum [72], vanadium [72]) exhibit a somewhat different behavior under these conditions. The measurement results of elastic precursor decay in high-purity tantalum are illustrated by way of example in Fig. 22. Despite a significant scatter in the experimental data, which is supposedly typical for bcc metals, measurements at room temperature clearly demonstrate a transition from the high-rate branch of the stress dependence of the deformation rate to the low-rate branch with precursor decay. This transition, of course, also manifests itself for fcc metals, but it takes place at a far lower stress in the elastic precursor. Unlike fcc metals, no anomalous increase in the Hugoniot elastic limit with temperature is observed in this case. The observed lowering of the Hugoniot elastic limit with heating is especially significant for specimens thicker than a 1 mm; for thin samples, the temperature effect turns out to be small. A small temperature dependence was also obtained in the molecular dynamics simulations [84] of dislocation motion at stresses higher than the Peierls stress; at a lower stress, the dislocation motion is distinctly thermofluctuational in nat-

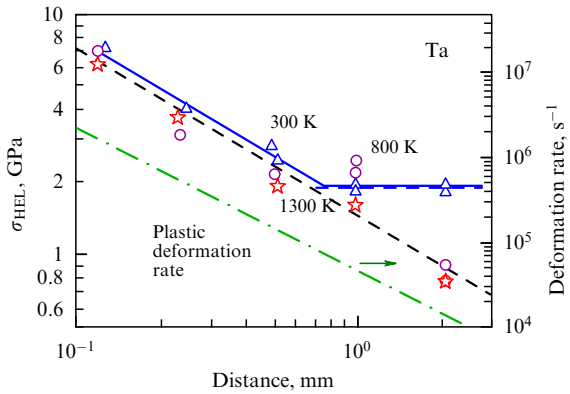

Figure 22. Elastic precursor decay in tantalum [72] at normal and elevated temperatures.

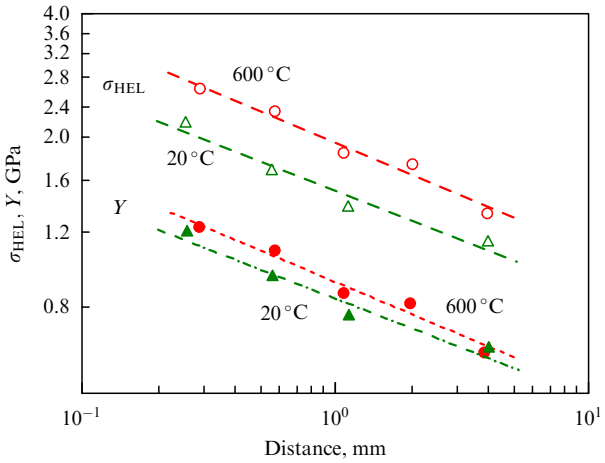

Figure 23. Elastic precursor decay in a VT1-0 titanium specimen at normal and elevated temperatures [73]; σ_{HEL} is the Hugoniot elastic limit equal to the compression stress in the elastic precursor, and Y is the plastic flow stress.

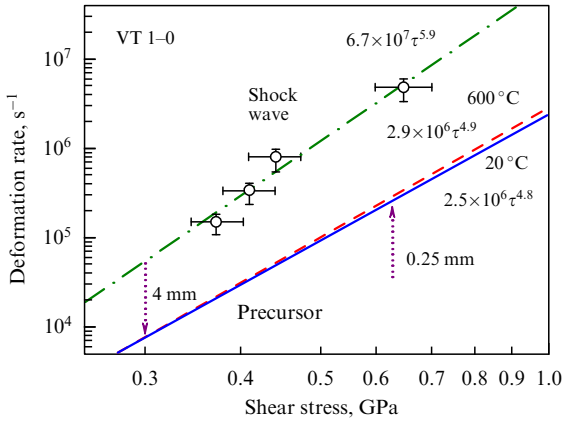

Figure 24. Dependences of the plastic deformation rate on the shear stress in the elastic precursor for VT1-0 titanium at normal temperature (solid line) and at 600 °C (dashed line) [73]. Vertical lines indicate the boundaries of the investigated parameter domain. Circles connected with a dashed–dotted line stand for the deformation rate in a plastic shock wave [36].

ure. Considering the resistance to dislocation motion as the sum of the contributions from the Peierls stress and the phonon viscosity, the weak temperature dependence may be represented as a result of opposite temperature effects in these constituents.

Metals with the fcc structure are usually less ductile and in pure form are prone to forming a coarse-grain structure, which impedes performing experiments of this kind. To date, experimental data have been obtained only for alloys (or metals with impurities) and single crystals.

Figure 23 gives the results of measurements [73] of elastic precursor decay in annealed VT1-0 commercial titanium specimen. One can see from the plot that the Hugoniot elastic limit is somewhat higher at an elevated temperature. However, this increase is insignificant and the values of the flow stress calculated from these data with the inclusion of the temperature dependences of elastic modulus turn out not to be very sensitive to the temperature. Figure 24 compares the dependences of the deformation rate on stress in the elastic precursor and in the plastic shock wave. As with other metals, the deformation rate in the plastic shock wave turns out for the same shear stress to be higher by about an order of magnitude than the initial plastic deformation rate in the elastic precursor. In the after-rolling state [36], the precursor decay is weak and, across all the distances traversed by the wave, the Hugoniot elastic limit remains almost invariable and corresponds to the HEL value in the annealed material at a long distance, while the compression rate in the plastic shock wave is about the same as in the annealed material.

3.3 Behavior of single crystals under shock-wave loading

Shock-wave investigations of elastoplastic strains and the fracture of single crystals occupy a special place, because they permit separating the contributions from different mechanisms of initiation and development of plastic strains and fracture. For obvious reasons, experiments on single crystals are not numerous. It is likely that they were performed mostly on metals with a close-packed hexagonal structure: beryllium [85], zinc [86, 87], and magnesium [88, 89]. Also investigated were the single crystals of metals with a body-centered cubic structure — molybdenum [90] and tantalum [91, 92] — and with a face-centered cubic structure: copper [93] and aluminum [47, 94].

Compared in Fig. 25 are the wave velocity histories for aluminum in different states at normal and elevated temperatures. The Hugoniot elastic limit of aluminum is not high and

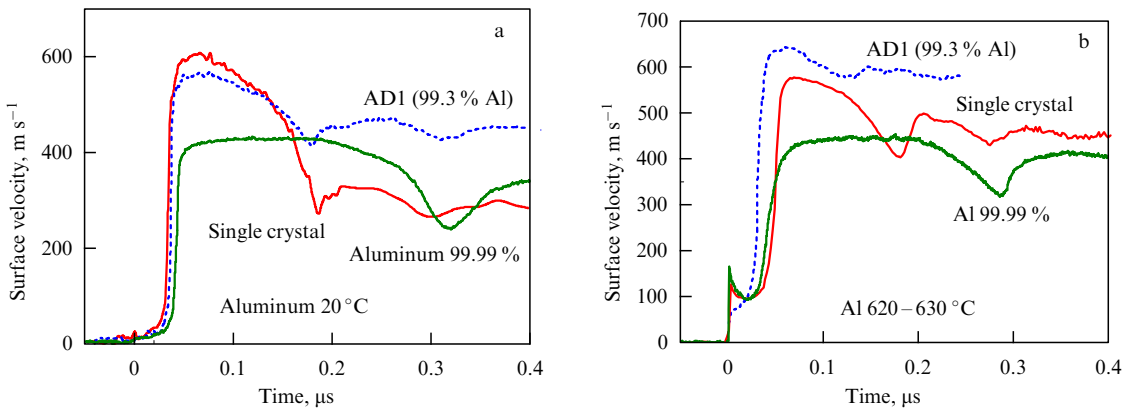

Figure 25. Comparison of the free surface velocity histories for AD1 commercial aluminum, single-crystalline aluminum, and high-purity polycrystalline aluminum at room temperature (a) and 620–630 °C (b) according to the data from Refs [33, 47, 80]. Specimen thicknesses: 2–3 mm.

no difference is seen on this scale in relation to the structural state at room temperature. A single crystal without large inclusions that might become fracture nuclei exhibits the highest resistance to spall fracture. The spall strength of high-purity polycrystalline aluminum is somewhat lower, while commercial aluminum is characterized by an even lower spall fracture stress. At a high temperature, the elastic precursor wave amplitude and, accordingly, the Hugoniot elastic limit are many times higher. In this case, in pure polycrystalline aluminum and in the single crystal, a characteristic stress peak forms at the precursor front, which testifies to a quickening stress relaxation, while in the case of commercial aluminum the precursor amplitude turned out to be somewhat lower, and its shape was the same as at room temperature. The relaxation quickening is supposedly a result of intense multiplication of dislocations. In commercial aluminum there is, evidently, an additional possibility of nucleating new dislocations on impurity particles. The spall strength near the melting temperature lowered for all three materials, to the greatest extent for commercial aluminum, which is supposedly due to the onset of grain-boundary melting at a temperature below the thermodynamic melting point of aluminum [55].

For a high symmetry of the fcc lattice, it is hard to expect large variations in the strength characteristics of crystals in relation to the direction of shock loading. In this respect, the most interesting results were obtained in experiments on hcp crystals. Cited below are some results of experiments [88] on the single crystals of magnesium.

The deformation mechanism of magnesium comprises three well-known slip systems: primary basal, prismatic, and pyramidal. When the basal slip is suppressed, a significant contribution to the plastic deformation is made by twinning. it is significant for shock-wave measurements that the possibility appears to study plastic flow in each system separately by varying the direction of wave propagation relative to the crystal axes. The primary basal slip should be observable for a shock compression in the direction inclined to the crystal c-axis. The secondary prismatic slipping is activated in the wave propagation in the direction perpendicular to the crystal symmetry c-axis, when there is no shear stress in the primary basal slip system. Lastly, the third, pyramidal, slip and twinning system should be activated in the propagation of the shock wave along the crystal c-axis.

Figure 26 compares the wave velocity histories measured in shock-wave loading in the directions of crystal c- and a-axes, and at an angle of 45° relative to the c-axis. The results of measurements clearly demonstrate the dependence of the Hugoniot elastic limit and spall strength on the direction of shock load application. As expected, the slipping along the basal plane (0001) takes place under the lowest value of the shear stress and exhibits the lowest value of the Hugoniot elastic limit in the shock compression.

Figures 27 and 28 demonstrate the temperature effect on the Hugoniot elastic limit of single-crystalline magnesium specimens of two orientations. It was expected that the forces of phonon viscosity might be comparable to the flow stress in the basal plane, which should result in an increase in the Hugoniot elastic limit with increasing temperature in the shock compression in an oblique direction. Experiments bear out this assumption. What was unexpected is an increase in the Hugoniot elastic limit with increasing temperature in the shock compression in the direction of the crystal c-axis, when the plastic deformation proceeds with the

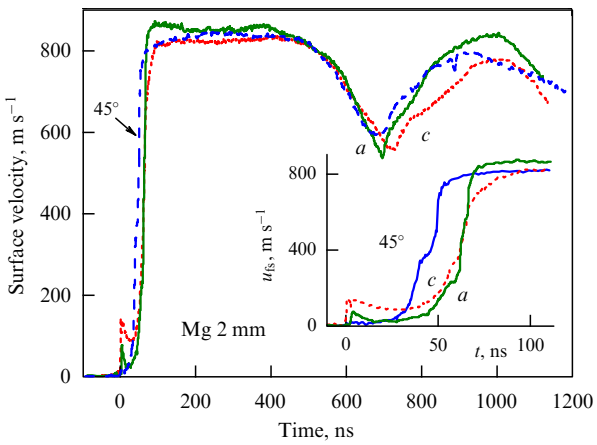

Figure 26. Free surface velocity histories for 2-mm thick single-crystalline specimens with three different orientations.

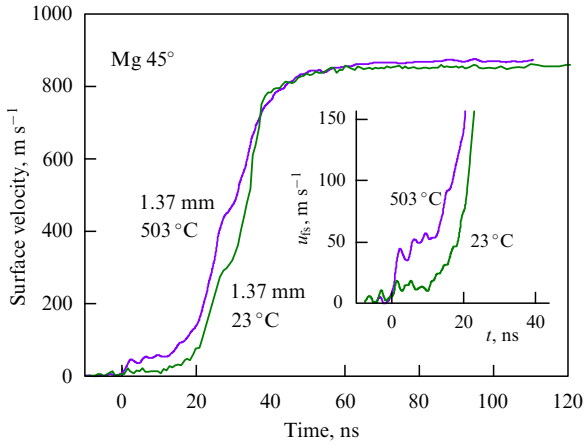

Figure 27. Free surface velocity histories for specimens with an orientation at an angle of 45° relative to the (0001) plane at normal and elevated temperatures.

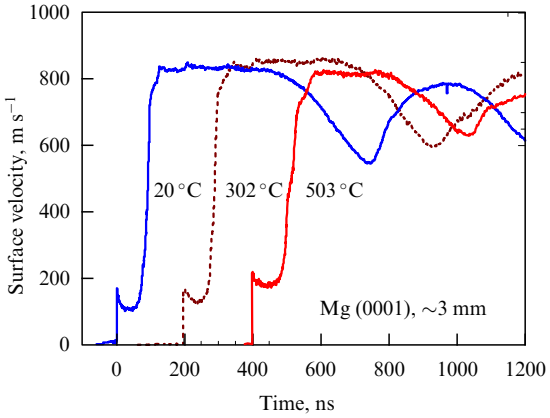

Figure 28. Free surface velocity histories for 3-mm thick specimens with (0001) orientation at normal and elevated temperatures.

participation of twinning and the flow stress is high. Calculations of the stress in the planes of plastic shear with the inclusion of the temperature dependences of elastic moduli show that the effect is much weaker, but in any case the high-rate plastic flow stress in all directions in the crystal does not decrease with heating.

An interesting feature of the presented wave velocity histories is the formation of two plastic waves in the

propagation through a relatively long distance. For load orientations along and across the crystal symmetry c-axis, an additional step in the profile of the plastic shock wave appears due to rereflections of the elastic precursor between the free surface and the plastic shock wave [5]. However, this explanation cannot be true for inclined-orientation specimens, where the Hugoniot elastic limit is too low. It should be noted that the splitting of the plastic shock wave in its propagation at an angle of 45° to the crystal axis, which was also observed in experiments on single crystals of beryllium [85], contradicts the theory of plane wave propagation through anisotropic elastoplastic media [95].

The formation of an additional step in the wave profile for the 45°-oriented specimen may be attributable to the activation of higher-order slip systems. For a uniaxial compression, the slip in inclined basal planes (0001) may furnish the relaxation of the longitudinal and one of transverse deviator stress components, but cannot result in the relaxation of the third component with the normal in the z-direction. For this reason, the stress difference $\sigma_x - \sigma_z$ continues to grow with compression, despite the fact that the slipping takes place in the (0001) plane and the secondary slip system should be activated when the stress difference $\sigma_x - \sigma_z$ becomes large enough.

If the two stress relaxation channels are activated one after the other, it is natural to assume that the first plastic shock wave would be similar to the elastic precursor as regards its definite propagation velocity and a weak dependence of its parameters on the final shock compression pressure. To elucidate the wave dynamics in the shock compression in an inclined direction, additional experiments were carried out with a varied shock compression pressure. The results are presented in Fig. 29. As is evident from these data, the higher the final shock compression pressure, the higher the parameters behind the first plastic wave. This feature of the wave dynamics was observed at the cracking of shock-compressed glass in failure waves [5]. The failure wave velocity is defined by the growth rate of cracks, depends only slightly on the pressure, and is not related directly to the material compressibility, whence it follows that the stressed state ahead of the failure wave is determined by the parameters of the state behind it. By analogy with the failure wave, it may be assumed that the additional 'step' in the wave profiles of inclined-orientation specimens is associated with the propagation of the crystal twinning front.

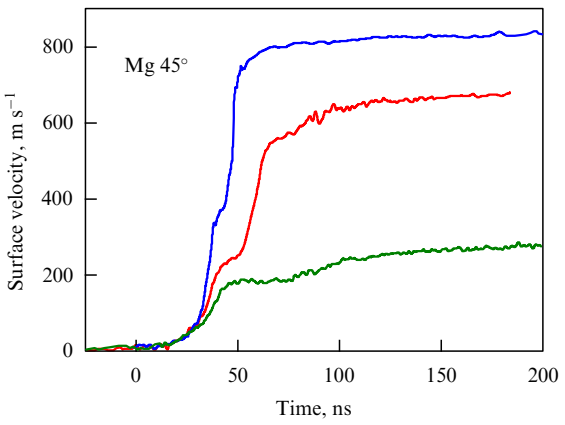

Figure 29. Free surface velocity histories for 2-mm thick specimens with a 45° orientation at different shock compression pressures.

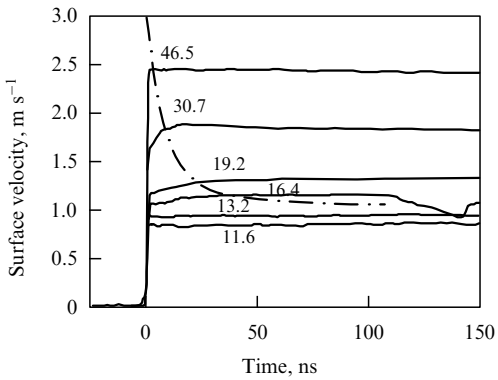

Figure 30. Free surface velocity histories for zinc specimens with thicknesses of 0.25–0.5 mm and ⟨0001⟩ orientation for different shock compression pressures [87]. The shock waves with a pressure over 30 GPa were generated by detonating an explosive charge in contact with the screen; realized in the remaining cases was the collision of plates. Indicated [in GPa] are the highest values of compressive stresses behind the shock wave front.

A wave configuration without an advanced elastic precursor, which is exotic for metallic materials, was observed in experiments on single-crystalline zinc [87] (Fig. 30). For a particle velocity of up to ~ 1 km s^{-1} (compression stress is about 14 GPa), the compression wave is practically a parameter jump with a rise time of no longer than 1–1.5 ns, followed by a domain with constant parameters. With an increase in shock compression pressure, a domain appears behind the shock front with a relatively smooth rise, whose duration shortens as the intensity of the shock wave becomes higher. It would be natural to assume that the appearance of this dissipative segment signifies the onset of plastic deformation in the shock wave. The shortening of the duration of the stress relaxation domain with an increase in shock compression pressure is evidently of the same nature as the commonly observable decrease in the width of plastic shock waves.

3.4 Dislocation multiplication effects

The strong stress dependence of the initial rate of plastic deformation behind the front of an elastic precursor contradicts the general stress dependence of the plastic flow rate expected for the high-rate branch shown in Fig. 1. The expectations were based on the Orowan formula (1), in which the dislocation velocity controlled in this mode by the phonon viscosity depends linearly on the stress, while the mobile dislocation density corresponds to the initial state of the annealed material and is a constant. The strong nonlinear stress dependences of the initial rate of plastic deformation behind the front of the elastic precursor and the unexpectedly high values of the rate itself may be treated as an evidence that the process is governed to a larger extent by the nucleation and multiplication of dislocations rather than by their velocity. It is likely that the nucleation and multiplication of dislocations may largely occur directly in the frontal part of the elastic precursor, in the course of compression, which is commonly considered as being purely elastic.

Figure 31 plots the initial portions of free surface velocity histories of two-millimeter thick pure copper specimens subjected to shock compression at different temperatures [71]. The authors call the reader's attention to the relatively long rise time at room temperature in the elastic part of the wave profile. In the analysis of precursor decay, the build-up

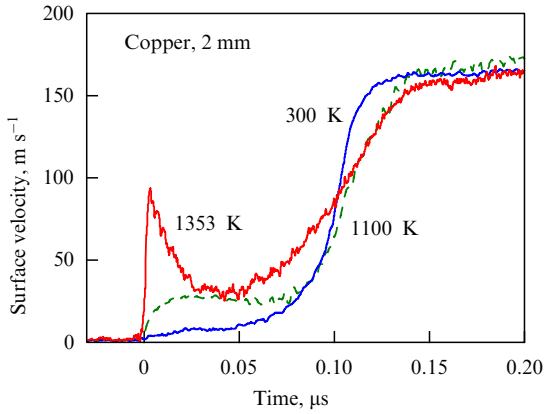

Figure 31. Variation of the Hugoniot elastic limit and the shape of the elastic precursor of a shock compression wave in pure copper upon increasing the test temperature [71]. The measurements were made for an impact velocity of 161 ± 8 m s^{-1} of the copper liner plate.

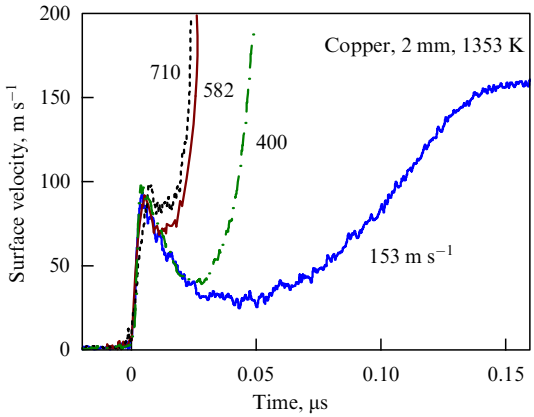

Figure 32. Free surface velocity histories of 2-mm thick copper specimens subjected to the impact of a copper plate with different velocities at a temperature of 1353 K [71]. The figures alongside the histories indicate the impact velocity [in m s^{-1}].

time is usually ignored, and this part of the wave is treated as a shock discontinuity; for a long build-up time, however, it is quite likely that the dislocation multiplication takes place even in the course of compression in the dispersed precursor front. With an increase in temperature and the corresponding rise in the contribution of phonon viscosity to the resistance to plastic deformation, the stress relaxation moderates, which manifests itself in an increase in precursor amplitude and rise time in the plastic shock wave. Owing to nonlinear effects, its rise time becomes shorter with an increase in compression stress in the elastic precursor: a sharp shortening of the elastic wave width near the melting temperature is also attended by a change in its shape. The stress peak in the frontal part usually appears due to acceleration of stress relaxation, for instance, as a result of intense dislocation multiplication. By comparing the wave profiles in Fig. 31, one may assume that the shortening of rise time shifts the intense multiplication to the domain immediately behind the elastic jump. At present, unfortunately, no wave theory in relaxing media is anywhere near complete that would establish a quantitative relation between the relaxation law and the wave evolution.

Figure 32 serves to illustrate an important feature of the evolution of elastic precursors with a stress peak in the frontal part. One can see that the parameters in the minimum point between the elastic and plastic waves increase upon increasing the impact velocity, while the recorded HEL magnitude remains practically invariable. The portion of the elastic precursor from its front to almost the minimum point is reproduced quite well, irrespective of the impact velocity. In other words, the mechanical perturbations from the plastic shock wave cannot pass through the minimum point and exert any effect on the frontal part of the elastic precursor.

From the measurement data on the evolution of elastic precursors in copper at a temperature of 1353 K [71], it was possible to estimate the rate of plastic deformation in the precursor at its different stages and then, using Orowan formula (1) and the data on the dislocation drag coefficient calculated in Ref. [96], estimate the mobile dislocation density variation. The results are demonstrated in Figs 33 and 34. These estimates show that the dislocation density increases by nearly an order of magnitude during the first 13–15 ns after compression at the front of the elastic precursor and then remains practically constant, while the state of the material

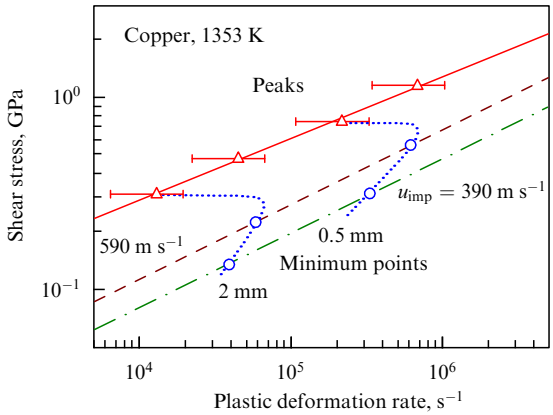

Figure 33. Relation between the rate of plastic deformation and the stress in the decayed elastic precursor in copper at a temperature of 1353 K [71]. The dotted lines connect the points of wave propagation distances equal to 2 and 0.5 mm. The dashed and dashed-dotted lines show the parameters at the minimum between the elastic and plastic waves for two different impact velocities u_{imp}.

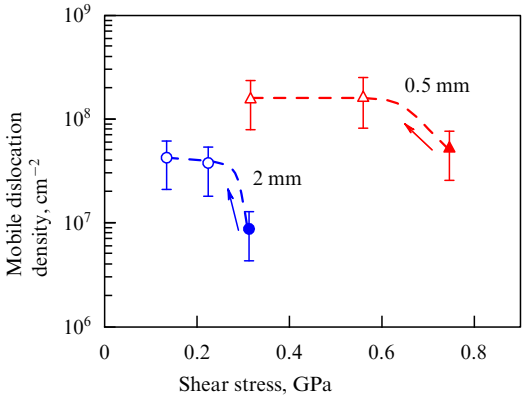

Figure 34. Mobile dislocation density as a function of shear stress, according to the data from Fig. 33. Solid symbols mark the parameters at the peak of the precursor. The arrows indicate the direction of parameter variation behind the stress maximum in the peak.

approaches the minimum point between the elastic and plastic waves. The plastic deformation itself amounts to about 0.1% during the first 13–15 ns. The termination of dislocation

multiplication with stress decreasing may be treated as evidence that the multiplication is controlled not only by the magnitude of deformation but also by the magnitude of the acting stress. The subsequent compression in the plastic shock wave is accompanied by an increase in shear stress and, as already noted, further dislocation multiplication.

Since the resultant experimental data give grounds to assume that significant dislocation magnification may occur even in the course of compression in the frontal part of the elastic precursor, it was natural to investigate the relationship between the rise time in the elastic precursor and the current value of the Hugoniot elastic limit, as well as the general evolution of the shock compression elastoplastic wave. Carried out in Ref. [97] for this purpose were experiments on vanadium, in which a compression wave was introduced into the samples through intermediate plates of different sorts of glass. The compressibility of silicate glasses behaves in an anomalous way, with the result that compression waves in these glasses increase their width during propagation.

Figure 35 compares the wave profiles measured for 0.5- and 2-mm thick specimens for three types of dynamic compression: shock, shockless, and mixed. The final compression stress was about the same in all three series. The mixed compression parameters are such that the transition from the shockless part to the shock-wave part occurs for a lower stress than the Hugoniot elastic limit at a long distance. Nevertheless, an increase in compression time in this series from 1–2 ns to about 150 ns did not result in a significant decrease in stress at the precursor peak. The parameters recorded at the peak for a 0.5-mm thick specimen in this case are even higher than in the shock compression; however, this is explained not by peculiarities of stress relaxation but by the wave dynamics of compression pulse reflection from the free surface [97]. On the other hand, in experiments with completely shockless compression, the stress at the precursor peak did become lower due to the lengthening of the rise time.

Of greater interest is the result of this series of experiments, shown in Fig. 36. It turned out that for all three versions of dynamic compression the parameters at the minimum point between the elastic and plastic waves evolved in practically the same way during propagation and could be approximated by the common functional dependence. This signifies that, despite the different deformation histories, the material approaches the minimum point with virtually the same mobile dislocation density.

The plot in Fig. 36 also demonstrates the previously unobserved nonmonotone character of the evolution of an elastoplastic shock compression wave in annealed vanadium. Elastic precursor decaying is caused by stress relaxation behind its front, but no relaxation process can result in a growth of stress in the wave during its propagation. A possible mechanism of stress growth at the minimum between the elastic and elastoplastic waves is suggested by a comparison of the wave profiles in Fig. 37, which clearly demonstrates the emission of a new elastic precursor by the plastic shock wave once it has traversed a distance longer than 2 mm. This signifies that the stress in front of the plastic shock wave has fallen below the material elastic limit in the course of precursor decay. The newly emitted elastic wave raises the pressure in front of the plastic shock wave to the current value of the Hugoniot elastic limit. In any case, the discovered nonmonotonicity is a consequence of a certain relation

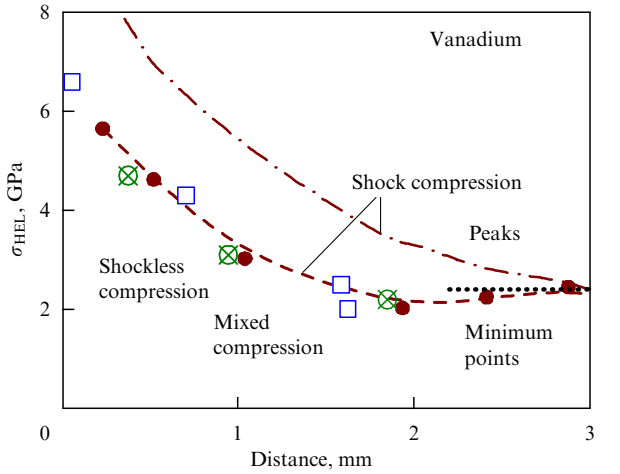

Figure 36. Decay of the elastic precursor in the shock, shockless, and mixed dynamic compression of vanadium. The symbols show the parameters at the minima between the elastic and plastic waves. The dashed-dotted line describes the decay of the precursor peak in the shock compression. The dotted line at the right shows the estimated magnitude of the HEL upon termination of precursor decay.

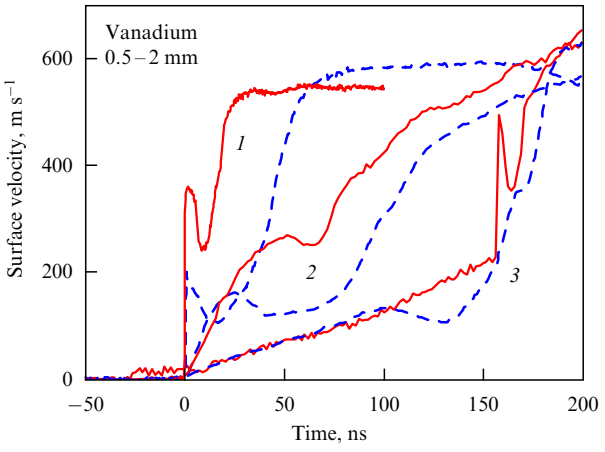

Figure 35. Free surface velocity histories of vanadium specimens with thicknesses of 0.5 mm (solid lines) and 2 mm (dashed lines) measured in the shock (1), shockless (2), and mixed (3) dynamic compression [97].

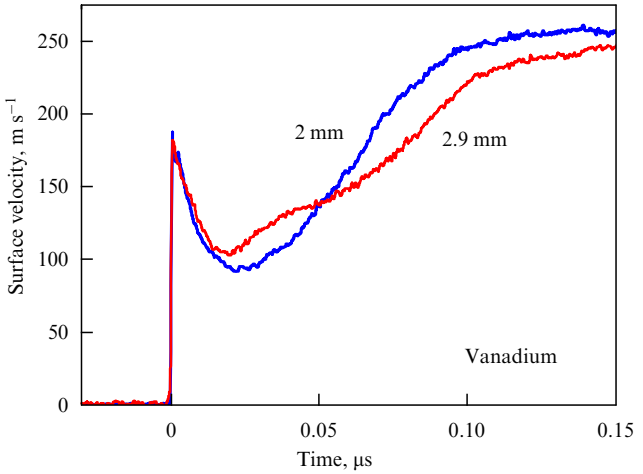

Figure 37. Free surface velocity histories of annealed specimens measured in Ref. [72] in the domain of nonmonotonicity of the evolution of a shock compression elastoplastic wave. The figures alongside the histories mark the specimen thickness.

between the contributions to the wave dynamics made by the multiplication of dislocations and stress relaxation caused by them. On the other hand, it is well known [98, 99] that a large contribution to the plastic deformation mechanism of vanadium is made by twinning. From this standpoint, the observed feature may be due to the fact that the nucleation of twins requires a significantly higher stress in the bulk of the material than their growth does.

4. Conclusions

The results of new experiments presented here confirm the informative value and fruitfulness of shock-wave investigations into the strength properties of materials under extremely high rates of loading. Recent years have seen a considerable broadening of the temporal range of the research, making it possible to perform measurements in fact at the limit of applicability of continuum mechanics and to enter the range of spatial and time scales that had earlier been dealt with only in the simulation of substance motion by the molecular dynamics method. The resultant new systematic data on the temperature-rate dependences of the resistance to high-rate deformation of metals with different crystal structures form the basis for the development of comprehensive, wide-ranging, constitutive relations required in the calculation of intense pulsed actions on materials and structures. The range of materials in which an anomalous rise in high-rate plastic flow stress is possible at elevated temperatures has been determined. New information has been obtained about the properties of multiplication of the elementary carriers of plastic deformation — dislocations — at the early stages of straining. Several specific features were discovered in the dynamics of elastoplastic shock compression waves in relaxing media, which are still imperfectly understood and call for a theoretical description. Unfortunately, no theory of the effect is anywhere near complete, which restricts the amount of information acquired by analyzing the dynamics of shock compression elastoplastic waves. The authors hope that their review will stimulate theoretical research in this area.

Acknowledgments
This work was supported by the Russian Science Foundation under grant No. 14-12-01127.

References

1. Fortov V E *Uravneniya Sostoyaniya Veshchestva: Ot Ideal'nogo Gaza do Kvark-Glyuonnoi Plazmy* (Equations of State of Matter: From Ideal Gas to Quark-Gluon Plasma) (Moscow: Fizmatlit, 2013)
2. Fortov V *Thermodynamics and Equations of State for Matter: From Ideal Gas to Quark-Gluon Plasma* (Singapore: World Scientific, 2016)
3. Clifton R J *Int. J. Solids Struct.* **37** 105 (2000)
4. Meyers M A et al. *Mater. Sci. Eng. A* **322** 194 (2002)
5. Kanel G I, Razorenov S V, Fortov V E *Shock-Wave Phenomena and the Properties of Condensed Matter* (New York: Springer, 2004)
6. Remington B A et al. *Mater. Sci. Technol.* **22** 474 (2006)
7. Kanel' G I, Fortov V E, Razorenov S V *Phys. Usp.* **50** 771 (2007); *Usp. Fiz. Nauk* **177** 809 (2007)
8. Lorenzana H E et al. *Sci. Modeling Simulations* **15** 159 (2008)
9. Vogler T J, Chhabildas L C *Int. J. Impact Eng.* **33** 812 (2006)
10. Asay J R et al. *J. Appl. Phys.* **103** 083514 (2008)
11. Brown J L et al. *J. Appl. Phys.* **114** 223518 (2013)
12. Jensena B J, Gupta Y M *J. Appl. Phys.* **104** 013510 (2008)
13. Turneaure S J, Gupta Y M *J. Appl. Phys.* **109** 123510 (2011)
14. Clifton R J *Appl. Mech. Rev.* **43** 5 S9 (1990)
15. Berner R, Kronmüller H "Plastische Verformung von Einkristallen", in *Moderne Probleme der Metallphysik: Erster Band Fehlstellen, Plastizität, Strahlenschädigung und Elektronentheorie* (Ed. A Seeger) (Berlin: Springer–Verlag, 1965) p. 35
16. Ninomura T *J. Phys. Soc. Jpn.* **36** 399 (1974)
17. Al'shits V I, Indenbom V I *Sov. Phys. Usp.* **18** 1 (1975); *Usp. Fiz. Nauk* **115** 2 (1975)
18. Nagornyi E M *Sov. Phys. Usp.* **5** 462 (1962); *Usp. Fiz. Nauk* **77** 201 (1962)
19. Zel'dovich Ya B, Raizer Yu P *Physics of Shock Waves and High-Temperature Hydrodynamic Phenomena* Vols 1, 2 (New York: Academic Press, 1966, 1967); *Fizika Udarnykh Voln i Vysokotemperaturnykh Gidrodinamicheskikh Yavlenii* (Moscow: Nauka, 1966)
20. Kanel' G I et al. *Udarno-Volnovye Yavleniya v Kondensirovannykh Sredakh* (Shock-Wave Phenomena in Condensed Media) (Moscow: Yanus-K, 1996)
21. Garkushin G V, Kanel' G I, Razorenov S V *Phys. Solid State* **54** 1079 (2012); *Fiz. Tverd. Tela* **54** 1012 (2012)
22. Duvall G E, in *Stress Waves in Anelastic Solids, Symp., Providence, R.I., April 3–5, 1963* (Eds H Kolsky, W Prager) (Berlin: Springer, 1964)
23. Asay J R, Fowles G R, Gupta Y *J. Appl. Phys.* **43** 744 (1972)
24. Chhabildas L C, Asay J R *J. Appl. Phys.* **50** 2749 (1979)
25. Swegle J W, Grady D E *J. Appl. Phys.* **58** 692 (1985)
26. Antoun T et al. *Spall Fracture* (New York: Springer, 2003)
27. Kanel G I *Int. J. Fract.* **163** 173 (2010)
28. Ashitkov S I et al. *JETP Lett.* **92** 516 (2010); *Pis'ma Zh. Eksp. Teor. Fiz.* **92** 568 (2010)
29. Whitley V H et al. *J. Appl. Phys.* **109** 013505 (2011)
30. Ashitkov S I et al. *AIP Conf. Proc.* **1426** 1081 (2012)
31. Gupta Y M et al. *J. Appl. Phys.* **105** 036107 (2009)
32. Winey J M et al. *J. Appl. Phys.* **106** 073508 (2009)
33. Garkushin G V, Kanel' G I, Razorenov S V *Phys. Solid State* **52** 2369 (2010); *Fiz. Tverd. Tela* **52** 2216 (2010)
34. Arvidsson T E, Gupta Y M, Duvall G E *J. Appl. Phys.* **46** 4474 (1975)
35. Sakino K *J. Physique IV* **10** (9) 57 (2000)
36. Kanel' G I et al. *Phys. Solid State* **58** 1191 (2016); *Fiz. Tverd. Tela* **58** 1153 (2016)
37. Kanel' G I et al. *High Temp.* **55** 365 (2017); *Teplofiz. Vys. Temp.* **55** 380 (2017)
38. Krüger L et al. *Int. J. Impact Eng.* **28** 877 (2003)
39. Kanel' G I et al. *Phys. Solid State* **45** 656 (2003); *Fiz. Tverd. Tela* **45** 625 (2003)
40. Kanel G I, Razorenov S V, Fortov V E *J. Phys. Condens. Matter* **16** S1007 (2004)
41. Kanel G I *Fatigue Fracture Eng. Mater. Struct.* **22** 1011 (1999)
42. Barbee T W et al. *J. Mater.* **7** 393 (1972)
43. Davison L, Stevens A L *J. Appl. Phys.* **43** 988 (1972)
44. Johnson J N *J. Appl. Phys.* **52** 2812 (1981)
45. Curran D R, Seaman L, Shockey D A *Phys. Rep.* **147** 253 (1987)
46. Kanel G I et al. *J. Appl. Phys.* **79** 8310 (1996)
47. Kanel G I et al. *J. Appl. Phys.* **90** 136 (2001)
48. Eliezer S, Moshe E, Eliezer D *Laser Part. Beams* **20** 87 (2002)
49. Utkin A V *J. Appl. Mech. Tech. Phys.* **34** 578 (1993); *Prikl. Matem. Tekh. Fiz.* **34** (4) 140 (1993)
50. Utkin A V *J. Appl. Mech. Tech. Phys.* **38** 952 (1997); *Prikl. Matem. Tekh. Fiz.* **38** (6) 157 (1997)
51. Kanel G I et al. *Int. J. Impact Eng.* **20** 467 (1997)
52. Zhakhovskii V V et al. *Appl. Surf. Sci.* **255** 9592 (2009)
53. Zhilyaev P A et al. *Phys. Solid State* **52** 1619 (2010); *Fiz. Tverd. Tela* **52** 1508 (2010)
54. Sin'ko G V, Smirnov N A *JETP Lett.* **75** 184 (2002); *Pis'ma Zh. Eksp. Teor. Fiz.* **75** 217 (2002)
55. Garkushin G V et al. *Int. J. Fract.* **197** 185 (2016)
56. Zaretsky E B, Kanel G I *J. Appl. Phys.* **112** 053511 (2012)
57. Kanel' G I et al. *JETP Lett.* **102** 548 (2015); *Pis'ma Zh. Eksp. Teor. Fiz.* **102** 615 (2015)
58. Zaretsky E B *J. Appl. Phys.* **120** 025902 (2016)
59. Ashitkov S I et al. *JETP Lett.* **103** 544 (2016); *Pis'ma Zh. Eksp. Teor. Fiz.* **103** 611 (2016)

60. Bogach A A, Utkin A V *J. Appl. Mech. Tech. Phys.* **41** 752 (2000); *Prikl. Matem. Tekh. Fiz.* **41** (4) 198 (2000)
61. Ashitkov S I et al. *J. Phys. Conf. Ser.* **500** 112006 (2014)
62. Kanel G I et al. *J. Appl. Phys.* **106** 043524 (2009)
63. Lang J M (Jr.), Gupta Y M *J. Appl. Phys.* **107** 113538 (2010)
64. McWilliams R S et al. *Phys. Rev. B* **81** 014111 (2010)
65. Ashitkov S I et al. *JETP Lett.* **98** 384 (2013); *Pis'ma Zh. Eksp. Teor. Fiz.* **98** 439 (2013)
66. Ashitkov S I et al. *JETP Lett.* **101** 276 (2015); *Pis'ma Zh. Eksp. Teor. Fiz.* **101** 294 (2015)
67. Vorob'ev A A, Dremin A N, Kanel' G I *J. Appl. Mech. Tech. Phys.* **15** 661 (1974); *Prikl. Matem. Tekh. Fiz.* **5** 94 (1974)
68. Clatterbuck D M, Chrzan D C, Morris J W (Jr.) *Acta Mater.* **51** 2271 (2003)
69. Ogata S et al. *Phys. Rev. B* **70** 104104 (2004)
70. Crowhurst J C et al. *J. Appl. Phys.* **115** 113506 (2014)
71. Zaretsky E B, Kanel G I *J. Appl. Phys.* **114** 083511 (2013)
72. Zaretsky E B, Kanel G I *J. Appl. Phys.* **115** 243502 (2014)
73. Kanel G I, Razorenov S V, Garkushin G V *J. Appl. Phys.* **119** 185903 (2016)
74. Zaretsky E B, Kanel G I *J. Appl. Phys.* **110** 073502 (2011)
75. Mashimo T, Hanaoka Y, Nagayama K *J. Appl. Phys.* **63** 327 (1988)
76. Arnold W, in *Shock Compression of Condensed Matter 1991. Proc. of the American Physical Society Topical Conf., Williamsburg, Virginia, June 17–20, 1991* (Eds S C Schmidt et al.) (Amsterdam: North-Holland, 1992) p. 539
77. Garkushin G V et al. *Mech. Solids* **45** 624 (2010); *Izv. Ross. Akad. Nauk. Mekh. Tverd. Tela* **45** (4) 155 (2010)
78. Razorenov S V et al. *Phys. Solid State* **54** 790 (2012); *Fiz. Tverd. Tela* **54** 742 (2012)
79. McClintock F A, Argon A S *Mechanical Behavior of Materials* (Reading, Mass.: Addison-Wesley, 1966); Translated into Russian: *Deformatsiya i Razrushenie Materialov* (Moscow: Mir, 1970)
80. Zaretsky E B, Kanel G I *J. Appl. Phys.* **112** 073504 (2012)
81. Olmsted D L et al. *Mater. Sci. Eng.* **13** 371 (2005)
82. Kuksin A Yu, Stegailov V V, Yanilkin A V *Dokl. Phys.* **53** 287 (2008); *Dokl. Ross. Akad. Nauk* **420** 467 (2008)
83. Zaretsky E B, Kanel G I *J. Appl. Phys.* **117** 195901 (2015)
84. Barton N R et al. *J. Appl. Phys.* **109** 073501 (2011)
85. Pope L E, Johnson J N *J. Appl. Phys.* **46** 720 (1975)
86. Bogach A A et al. *Phys. Solid State* **40** 1676 (1988); *Fiz. Tverd. Tela* **40** 1849 (1998)
87. Bezruchko G S, Kanel G I, Razorenov S V *Tech. Phys.* **50** 621 (2005); *Zh. Tekh. Fiz.* **75** (5) 92 (2005)
88. Kanel G I et al. *J. Appl. Phys.* **116** 143504 (2014)
89. Winey J M, Renganathan P, Gupta Y M *J. Appl. Phys.* **117** 105903 (2015)
90. Kanel G I et al. *J. Appl. Phys.* **74** 7162 (1993)
91. Asay J R et al. *J. Appl. Phys.* **109** 073507 (2011)
92. Whiteman G, Case S F, Millett J C *J. Phys. Conf. Ser.* **500** 112067 (2014)
93. Tonks D L et al. *J. Physique IV* **10** (Pr9) 787 (2000)
94. Huang H, Asay J R *J. Appl. Phys.* **101** 063550 (2007)
95. Johnson J N *J. Appl. Phys.* **43** 2074 (1972)
96. Kuksin A Yu, Yanilkin A V *Phys. Solid State* **55** 1010 (2013); *Fiz. Tverd. Tela* **55** 931 (2013)
97. Kanel G I et al. *J. Appl. Phys.* **118** 045901 (2015)
98. Chhabildas L C, Hill C R, SNL Report SAND-85-0322C (Albuquerque, NM: Sandia Natl. Lab., 1985)
99. Nemat-Nasser S, Guo W *Mech. Mater.* **32** 243 (2000)